LentiRILES, a miRNA-ON Sensor System for Monitoring the Functionality of miRNA in Cancer Biology and Therapy

Viorel Simion, Claire Loussouarn, Yoan Laurent, Loris Roncali, David Gosset, Flora Reverchon, Audrey Rousseau, Francisco Martin, Patrick Midoux, Chantal Pichon, et al.

LentiRILES, a miRNA-ON Sensor System for Monitoring the Functionality of miRNA in Cancer Biology and Therapy

Viorel Simion[1], Claire Loussouarn[2], Yoan Laurent[1], Loris Roncali[2], David Gosset[1], Flora Reverchon[1], Audrey Rousseau[2], Francisco Martin[3], Patrick Midoux[1], Chantal Pichon[1], Emmanuel Garcion[2†], Patrick Baril[1†*]

[1] Centre de Biophysique Moléculaire, CNRS UPR4301, Université d'Orléans, France
[2] Université d'Angers, Université de Nantes, Inserm, CRCINA, SFR ICAT, Angers, France
[3] GENYO, Pfizer/University of Granada/Andalusian Regional Government, Granada, Spain

* To whom correspondence should be addressed. Tel: +33 2 3825 5640; Fax: +33 2 3863 1517; Email: patrick.baril@cnrs-orleans.fr

† The authors wish it to be known that, in their opinion, the last two authors should be regarded as joint last Authors.

Abstract

A major unresolved challenge in miRNA biology is the capacity to monitor the spatiotemporal activity of miRNAs expressed in animal disease models. We recently reported that the miRNA-ON monitoring system called RILES (RNAi-inducible expression Luciferase system) implanted in lentivirus expression system (LentiRILES) offers opportunity to decipher the kinetics of miRNA activity *in vitro*, in relation with their intracellular trafficking in glioblastoma cells. In this study we describe in detail the method for production of LentiRILES stable cell lines and employed it in several applications in the field of miRNA biology and therapy. We show that LentiRILES is a robust, highly specific and sensitive miRNA sensor system that can be used *in vitro* as a single-cell miRNA monitoring method, cell-based screening platform for miRNA therapeutics and as a tool to analyze the structure-function relationship of the miRNA duplex. Furthermore, we report the kinetic of miRNA activity upon the intracranial delivery of miRNA mimics in an orthotopic animal model of glioblastoma. This information is exploited to evaluate the tumor suppressive function of miRNA-200c as locoregional therapeutic modality to treat glioblastoma. Our data provide evidence that LentiRILES is a robust system, well-suited to resolve the activity of endogenous and exogenously expressed miRNAs for basic research to gene and cell therapy.

Key words : miRNA, molecular imaging, RILES, glioblastoma, RNA therapeutics

Introduction

MicroRNAs (miRNAs) are a large family of small, non-coding RNAs that play critical roles in the post-transcriptional regulation of gene expression. MiRNAs are predicted to regulate more than half of all mammalian protein-coding genes and are involved in almost all developmental and cellular processes (1-3). The canonical pathway of miRNA biogenesis in animals is initiated by transcription of long primary miRNAs (pri-miRNAs) by RNA polymerase II (4). The pri-miRNAs are processed in the nucleus by the Microprocessor complex into pre-miRNAs, hairpin intermediates of approx. 70 nucleotides (5). Pre-miRNAs are transported to the cytoplasm by exportin-5, where they are further cleaved by Dicer (RNase III enzyme) into approx. 22-bp duplex molecules with short 3'overhangs (6, 7). One strand of the duplex, the guide strand, is selectively incorporated into the RNA-induced silencing complex (RISC) containing the Argonaute (Ago) protein. The other strand, the passenger strand, is discarded. This class of non-coding RNAs bind to their target mRNAs by base pairing with partially complementary sequences in the 3'-untranslated region (3'UTR). Binding of miRNAs to target mRNAs results in translational repression and/or mRNA degradation (8-11). Each miRNA is believed to regulate up to several hundred targets, making up extensive gene expression regulatory networks (12). This evolutionarily conserved type of interaction between miRNAs and mRNAs has attracted great attention in the field of RNA biology and therapeutics (13). MiRNAs fulfil their biological function through a dynamic spatiotemporal expression pattern that fine-tunes the expression of multiple mRNA targets and collectively orchestrate biological responses (14-17). Beyond the well-illustrated spatiotemporal expression pattern of Lin 4 and let 7 miRNAs during embryonic development (18-23), there are many other miRNAs that are dynamically regulated during disease progression (24-26). For example, the miRNA-10b plays a role in the late stage of the metastatic process whereas it has a negligible effect in the first stage of tumour development (27) In preclinical therapeutic studies it was observed that the duration of gene silencing of therapeutic RNAi oligonucleotides is also variable and their biological activity depends on many parameters such as accessibility to the tumour site, diffusion trough tumour-microenvironment, proliferation rate of tumour cells and the half-life of mRNA targets (28-30). A better understanding of the dynamic expression pattern of miRNAs as well as miRNA delivery kinetics would be an advantage to better understand the functionality of miRNA and to optimize the benefits of miRNA-based therapeutics.

To resolve the spatiotemporal dynamics of miRNA-mediated gene regulation, it is necessary to assess the kinetics of miRNA expression in targeted cells or tissues. Expression levels of miRNA can be analysed by northern blotting, quantitative PCR, microarrays, and deep sequencing. However, kinetic analysis is laborious due to the need to collect samples at multiple time points. Furthermore, these methods fail to capture information on cell-to-cell variations in miRNA expression. Non-invasive molecular imaging modalities have the potential to fulfil these limitations. There are several miRNA molecular imaging methods developed to monitor the expression of miRNAs in real time and non-invasively. Molecular beacons which typically consist of stem-loop DNA oligonucleotides complementary to a miRNA strand, a fluorophore, and a quencher—overcome some of these limitations (31-33). However, signals of molecular beacons arise from hybridization of mature miRNA to stem-loop DNA, regardless of Ago2 loading. Thus, molecular beacons do not discriminate between Ago-loaded functional miRNA and free, non functional miRNA. Because miRNA expression levels do not necessarily correlate with miRNA activity, the miRNA functionality cannot be inferred from expression analysis alone (34). Moreover, the dilution of the probes over the cell division rate of the biological systems studied is a limitation for the longitudinal analysis of miRNA expression. To directly measure miRNA activity, luciferase reporter gene with miRNA target sequences in their 3'UTR have been widely used as miR-OFF reporter assays, and are also successfully utilized for bioluminescent imaging *in vivo* (34, 35). Consequently, the expression of miRNA is negatively signed by the loss of optical signal, a readout that is somewhat constraining as the absence of signal in molecular imaging can have different causes such as cell death, low resolution capacity or equipment dysfunction. The miR-ON gene reporter methods tackle some of these limitations. These systems rely on engineering of genetic-switch expression systems to induce optical signal in cells when the miRNA of interest is expressed and, importantly, functionally processed by the RISC machinery. Pichard et al., (36), Amendola et al., (37) and more recently Rossetti et al. (38) engineered the Tetracycline-Inducible tTR-KRAB System and revealed the temporal dynamic expression pattern of miRNAs in several type of cells *in vitro*. However the principle of regulation of this miR-ON system requires several hours to days for the tTR-KRAB regulator protein (39-41) to switch-ON the inducible expression cassette. Furthermore, KRAB-mediated silencing can act over several tens of kilobases and thus might affect the biology and behaviour of cells (42, 43). We previously designed the RILES system (RNAi-Inducible Luciferase Expression System) for spatiotemporal detection of miRNA activity in vivo by engineering the Cumate

genetic-switch operon (44-46) and, more recently, the Tetracycline genetic-switch operon systems in the Tet R configuration (47). We demonstrated that RILES switched ON the expression of luciferase and the hNIS reporter genes in a specific and dose-dependent manner and provided a temporal and spatial resolution of miRNA regulation *in vitro* and *in vivo*, that conventional detection methods can hardly achieve (45, 46). More recently (47), we demonstrated that subcloning the RILES in a lentiviral expression system provides the opportunity to monitor in real time and over short period of time the fate of miRNA activity in glioblastoma cells. We demonstrated that the time frame for the LentiRILES to be accurately switched-ON in cells is indeed rapid, starting 3 hours after transfection. When combined with confocal microscopy studies, this miR-ON monitoring system enabled us to decipher the critical steps of miRNA internalization, processing and exocytosis in U87MG glioblastoma cells (47).

Here, we fully characterized the LentiRILES in cells by challenging the sensitivity, specificity and robustness of this miRNA-ON monitoring system using several cell types. We employed lentiRILES to visualize miRNA regulation in single-cells, as a cell-based miRNA screening platform and as rationale to perform structure-function analysis of the miRNA duplex. We report, for the first time to our knowledge, the kinetic of miRNA-mediated mRNA silencing activity in a preclinical animal model of glioblastoma after the locoregional infusion of synthetic miRNA by convection-enhanced delivery. We exploit the bioluminescence data generated by lentiRILES system to evaluate the tumour suppressive function of miRNA-200c as a locoregional treatment of glioblastoma.

Methods

Tissue Culture and Reagents.

The U87MG, HEK 293 T, Hela, B16F10, 4T1 and C2C12 cell lines were purchased from ATCC (American Type Culture Collection) and maintained in culture according to standardized conditions. Cells were mycoplasma-free as evidenced by the MycoAlert Mycoplasma Detection Kit (Lonza). The commercial transfection reagents and synthetic miRNAs were purchased from several companies as indicated in the text. The polybrene (hexadimethrine bromide) used to increase lentiviral transduction efficiency and proteinase K

were from Sigma. The Tet R (clone 17795) and Argonaute 2 antibodies were from Abcam (Abcam, USA). The luciferin substrate for *in vitro* and *in vivo* use was from Promega. Our home-made lipopolyplexe transfection reagent, LPRi, was prepared as described recently (47).

Lentiriles Stable Cell Line Production and Selection.

The LentiRILES harbouring the CMV-TetO regulatable cassette encoding the luciferase reporter gene and the spleen focus-forming virus promoter driving the expression of the Tet R repressor gene originated from the Francisco Martin laboratory (GENYO, Pfizer/University of Granada, PTS Granada, Spain) and derived from a previous publication (48) . Procedures to place the Tet R transcriptional repressor under control of miRNA of interest as well as the protocol to produce the LentiRILES cell lines were the same as described recently (47) and according to conditions indicated in the text. The screening procedure to identify the LentiRILES cell lines that were the most responsive to miRNA of interest was carried out 7 days post-infection with the LentiRILES viral particles and by transfecting the cells with miRNA mimic at a final concentration of 100 nM using our LPRi lipopolyplexes transfection reagent.

Mirna Mimics Transfections and Luciferase Assay.

The transfection procedure to evaluate the potency of commercially available synthetic miRNA mimic and transfection reagents was performed strictly according to manufacturer's recommendations. At the indicated time point post transfection, the relative luciferase activity units (RLU) in wells were quantified using a luminometer equipped with automatic injectors and normalized to protein content (RLU/mg protein) as previously described (45). Alternatively, tissue culture plates were scanned using an IVIS Lumina II imaging scanner (PerkinElmer) after renewing the tissue culture media with determined from a standard procedure as previously described PBS containing the luciferin substrate at a final concentration of 150 µg/ml. The plates were scanned for 2 min. Light emission from regions of interest (ROI) was drawn manually and quantified as photons/second/pixel/sr using the living Image Software (PerkinElmer).

Quantitative Real-Time PCR.

The relative expression of Tet R and Luciferase mRNA as well as miRNAs was determined from a standard procedure as previously described (45). Briefly, short and long RNAs were collected simultaneously using the miRNAVANA isolation kit (ThermoFisher) then reverse-transcribed using the NCode VILO miRNA cDNA synthesis kit according to the manufacturer's instructions (ThermoFisher). Real time quantitative PCR was performed with SYBR green dyes (QuantiFast SYBR Green master mix, Qiagen) using specific Tet R (forward 5'-GCCCAGAAGCTAGGTGTAGA and reverse 5'-TGTACTTTTGCTCCATCGCG), luciferase (forward 5'-TCATAGAACTGCCTGCGTGA and reverse 5'- AGCAGCGCACTTTGAATCTT), E-caherin (forward 5'-CGTACATGTCAGCCAGCTTC and reverse 5'-TGGAGGAATTCTTGCTTTGC), Vimentin (forward 5'-TGTCCAAATCGATGTGGATGTTTC and reverse 5'-TTGTACCATTCTTCTGCCTCCTG), Zeb-1 (forward 5'-TTTCTTGCCCTTCCTTTCTG and reverse 5'-GGGAGGAGCAGTGAAAGAG) and Zeb-2 (forward 5'-CCACACTCTGTGCATTTGAACT and reverse 5'-AAGCCAGGGACAGATCAGC) primers and commercially available primers to miRNA-122, -133a, and -21.5 (Qiagen). The specificity of the PCR amplicon (size and product) and absence of primer-dimer were verified by melt-curve analysis using LightCycler 480 equipment and software (Roche). Samples were normalized to the GAPDH level for quantification of the mRNA transcripts and to the snU6 level for quantification of miRNA. Finally, the relative levels of expression of mRNAs and miRNAs were determined using the $2^{-\Delta\Delta Ct}$ method. To quantify the number of lentivirus vector copies integrated per genome, genomic DNA was extracted by lysing 10^6 cells in the SNET buffer (20 mM Tris-HCl pH 8, 5 mM EDTA pH 8, 400 mM NaCl, 1% SDS) containing proteinase K used at a final concentration of 100 mg/ml. After a phenol–chloroform extraction step to remove proteins, the genomic DNA was ethanol precipitated and quantified by spectrophotometry. Then 50 ng of extracted genomic DNA samples were used in each quantitative PCR reaction performed in triplicate using the Tet R and luciferase primers. The vector copy number (v.g.c) per host-cell genome was determined by interpolation to a standard curve prepared from serial dilution of the Tet R and Tet-o-Luc plasmids. Data were finally expressed as v.g.c value by assuming that 50 ng of genomic DNA is equivalent to 8 334 genomes as described previously (48).

Mirna Labelling and Confocal Microscopy Analysis.

For confocal microscopy studies of the intracellular distribution of transfected miRNAs in cells, miRNA mimics were labelled using the Label IT nucleic acid labelling kit according to the manufacturer's protocol (Mirus, USA) with some modification as described recently (47). After plating, the cell monolayers were transfected with LPRi complexed with 50 nM final concentration of Cyanine 3 (Cy-3)-labelled blunt or overhang miRNA-133a mimics for 6 hours in tissue culture. The cells were thereafter fixed in 3% paraformaldehyde/PBS solution at room temperature, washed and stained with the Argonaute 2 antibody overnight at 4°C. Coverslips were collected, mounted in Vectashield medium for fluorescence (H-100, Vector Laboratories) and analysed using the Zeiss LSM 510 confocal laser scanning microscope with an apochromat 63×/1.4 oil differential interference contrast (DIC) objective (Carl Zeiss). Colocalization analysis was monitored using the ImageJ plug-in JACoP (Just Another Co-localization Plugin). Each coloured image was split into respective red and green channels. The Mander's R coefficient was calculated based on the red and green channels. Final data were expressed as the co-localization coefficient, r2, from three independent experiments collected from a minimum of 50 independent cells per condition each time.

Cell Viability Assay, Cell Cycle and Apoptosis Flow Cytometry Analysis and In Vitro Wound Scratch Assay.

Cell viability upon transfection of miRNA-200c in U87MG cells was performed using the Alamar Blue assay following the manufacturer's recommendations (Sigma-Aldrich). Briefly described, at the time of the assay, the Alamar Blue stock solution was directly loaded in the tissue culture plate at a final dilution of 1/10 and incubated for 90 min at 37°C, 5% CO2. The plates were thereafter read using a fluorescence-based plate reader with a fluorescence excitation wavelength of 540–560 nm and an emission wavelength of 590-610 nm. The raw fluorescence values were corrected by subtracting the background fluorescence values detected in wells treated in the same condition but without cells. Fluorescence cell cycle analysis was performed by incubating 10^6 cells in suspension with 3 mL of 70 % ethanol followed by an incubation period of 1 hour at -20 °C. Ethanol was removed after centrifugation and total RNA discarded by treatment for 30 min at 37°C with RNAse A solution (ThermoFisher) used at the final concentration of 500 U/ml. The pellets were washed

twice in DPBS, resuspended in 300 µL of DPBS containing 0.2% Triton X-100 and analysed using Becton Dickinson FACSort (Becton Dickinson) after addition of propidium iodide solution used at the final concentration of 10 ng/µL. Fluorescence was collected from 30 000 events and analysed using the CellQuestTM Pro software (Becton Dickinson). Cell death and apoptosis analysis were performed after staining cells with a combination of Annexin V conjugated FITC and propidium iodide (ANNEX300F kit, Bio-Rad). Cells in suspension were first resuspended in binding buffer provided by the Annexin V:FITC Assay Kit before adding 5 µL of Annexin V conjugated FITC solution to 3 10^5 cells for 10 min of incubation at room temperature in the dark. Then propidium iodide was added to the cell suspension at a final concentration of 1 ng/ml before analysing the cell population by flow cytometry using the Becton Dickinson FACSort. A minimum of 30 000 events were acquired and analysed using CellQuestTM Pro software. *In vitro* wound scratch assays were performed by culturing the U87MG cells in 24-well plates to reach a nearly confluent cell monolayer the following day. The miRNA-200c mimics formulated with the LPRi transfection reagent were transfected to cells according to the protocol described above. Then 3 days later, vertical wounds were performed with sterile 20-200 μl plastic pipette tips. The plates were placed in a time lapse videomicroscope (Zeiss) placed in an environmental chamber at 37 °C, 5% CO2. Pictures of the wounds were recorded automatically every 2 hours for a total of 3 days. Wound areas at individual time points were measured using the ZEN LE Digital Imaging Software (Zeiss). Data were expressed as % of closure by normalizing the calculated area to 100 % of wound area of untreated cells.

Orthotopic Glioblastoma Animal Model and Locoregional Delivery **of LPRi Mimic.**

All mouse experiments were carried out in strict accordance with the rules of the French Ministry of Agriculture and the European Communities Council Directive (86/609/EEC). The experimental protocol used in this study was approved by the "Pays de la Loire" Ethics Committee of Animal Experiments (Permit No. CEEA. 2012.60; Authorization n°A 49-2012-04). Female CB-17/Icr-Prkdc scid/Rj mice (7 weeks old, Janvier Labs, France) were maintained in pathogen-free conditions with controlled temperature (20-22°C), humidity (50-70%), light (12 h light/dark cycles) and housed with unlimited access to food and water. Tumour implantations were done by stereotactic surgery according to detailed

procedures recently described (47) (49). The miRNA mimics (2 µg miRNA mimic formulated in 7 µl of PBS using a 10 fold concentrated LPRi solution) were infused into solid tumours by the convection-enhanced delivery method (CED). The CED infusion was performed using syringes equipped with a 32-G needle connected to the Harvard apparatus Pump and carried out automatically at a constant flow rate of 0.5 µL/min over a period of time of 18 min. After injection, the needles were left in place for an additional 5 min and gradually removed over an additional period of 5 min. The mice were monitored daily for mobility, grooming and weight.

Bioluminescence Imaging.

Bioluminescence imaging was performed rigorously as previously described (45) (47). The Living Image Software (PerkinElmer, USA) was used to express the data as photons/second/pixel/sr monitored from region of interest covering the brain of mice after a 2 min integration time with the following acquisition parameters: relative aperture F/Stop = 1, binning of 4, field of View D. The sensitivity of the imaging scanner was tested monthly with commercially available positive sources of bioluminescence.

MRI Imaging

MRI of mice was performed according to procedure described previously (49). Briefly, mice were isoflurane-anesthetized and scanned using a Burker Biospec 70/20 device, operating at a magnetic field of 7T (Bruker, Wissembourg, France), equipped with a 1 H cryoprobe. Anatomical proton images were generated using a acquisition with relaxation enhancement (RARE) sequence [TR = 3200 ms; mean echo time (TE) = 21.3 ms; RARE factor = 4; FOV = 2 cm x 2 cm; matrix 256 x 256; 11 contiguous slices of 0.5 mm, Nex = 1]. For monitoring tumour development overtime, a total of 8 MRI slices by brain were taken during the imaging session. Then regions of interest covering visible tumours areas were drawn using Paravision 6.0.1 software, summed and multiplied by the slice thickness to obtain the tumour volume at each time point and for each group of mice.

Statistical Analysis.

The results were expressed as mean ± S.E.M. and all the experiments were performed at least in triplicate. Statistical evaluation was carried out by one-way analysis of variance between groups (ANOVA program of Origin, OriginLab, Northampton, MA) or Student's t-test for comparisons between two groups. Statistical significance for survival experiments in animal was determined using the log rank test. Differences were considered to be statistically significant when $p < 0.05$.

Results and Discussion

Strategy of Production of LentiRILES Cell Lines

Recently, we engineered the Tet R-based lentiviral system developed by Benabdellah et al. (48) to produce a U87 MG stable cell line expressing the miR-ON RILES system constitutively (LentiRILES, Figure 1A). The system is based on two lentiviral vectors, one expressing the Tet R through the spleen focus forming virus (SFFV) promoter (Lenti Tet R) and the other expressing the firefly luciferase (FLuc) driven by the regulatable inducible CMV-Tet O promoter (Lenti Tet_O_Luc). We subcloned 4 complementary block sequences to a miRNA of interest (miR T cassette) downstream to the WPRE viral gene of the Lenti Tet R vector to place the expression of the Tet R repressor under control of the miRNA (Figure 1A). When the given miRNA is expressed in cells, it will bind to the miR T cassette, activating the RISC machinery and inhibiting the production of the Tet R protein. Consequently, in the absence of the Tet R protein bound on the Tet O operator, the inducible promoter is switched-ON, resulting in the expression of the FLuc and emission of a positive bioluminescence signature in cells that can be easily collected using a bioluminescence imaging scanner (Figure 1A). To achieve a high signal-to-noise ratio readout, we placed RILES under the control of miRNA-133a (LentiRILES/133T), a muscle-specific miRNA that is highly enriched in cells from cardiac and skeletal muscles lineages and undetectable in most other cell types derived from different organ sources (Figure 1B). Therefore, as illustrated in Figure 1A, in the presence of transfected miRNA-133a, the RILES system will be switched-ON in cells resulting in emission of bioluminescence signals that can be monitored using standard bioluminescence imaging scanner.

We challenged the LentiRILES/133T system by evaluating the responsiveness of the LentiRILES produced in several cancer cell lines, derived from different tissue origins, such as human cervical cancer (HeLa) cells, murine melanoma (B16F10) cells, mouse mammary carcinoma (4T1) cells and, for comparison, the human glioblastoma U87MG cell line (U87MG). We first developed and optimized the procedure to generate optimal-responsive LentiRILES/133T stable cell lines to the miRNA-133a used as the inducer of the OFF-to-ON shift of the RILES configuration. The general procedure (Figure 1C) consists in the transduction of cells with first a MOI value of the Lenti Tet R/133T viral particles to transfer expression of the Tet R protein in at least 80 % of the whole cell population. Then, 4 days later, cells were infected with different MOI values of the Lenti Tet_O_Luc viral particles to find an appropriate balance between expression of the Tet R protein and the number of Tet O operator sequences integrated in the host genome of cells.

To rationalize the best MOI values of Lenti Tet R/133 and Lenti_o_Luc viral particles, we first evaluated the transduction efficiency of each cell line using a lentivirus encoding for the eGFP reporter gene. Flow cytometry analysis of cells transduced at a MOI of 12.5 indicated (Figure 1D) that the most permissive cell line was the U87MG (80 % of GFP positive cells), followed by the HeLa cells (63 % of GFP positive cells), the B16F10 cells (35 % of GFP positive cells) and finally the 4T1 cells (35 % of GFP positive cells). According to this result, we selected for each cell line an appropriate MOI value of Lenti Tet R/133T viral particles to transfer expression of the Tet R protein in 70 % of the whole cell populations. We then infected the cells with increasing MOI values of Lenti Tet_O_Luc viral particles to find the best ratio of infection between the Lenti Tet R/133 and Lenti_o_Luc viral particles. We produced a total of 16 LentiRILES/133T cell lines and evaluated their responsiveness to miRNA-133a transfected in 96-well plates using a bioluminescence imaging scanner. The results demonstrate that all the LentiRILES/133T stable cell lines generated were responsive to the miRNA-133a mimic with however different efficiency (Figure 1E). Quantification of bioluminescence signals emitted from the cells indicated that a Lenti Tet R 133T to Lenti Tet_O_Luc MOI ratio of 2/1 was the best ratio to generate optimal-responsive cells to miRNA-133a. As show in Figure 1E, Hela cells transduced with a MOI ratio of 30/15 had a maximum 5.8-fold increase in luciferase activity in response to transfected miRNA-133a, while the B16F10 melanoma cells transduced with a MOI ratio of 50/25 had a maximum 3.1-fold increase of luciferase activity. The 4T1 breast cancer cells

were found to be the less responsive LentiRILES/133T cell line as a maximum 2.2-fold increase in luciferase activity was detected in these cells for a MOI ratio of 50/25. In contrast, the U87MG glioblastoma cells were the most responsive cell line to transfected miRNA-133a as a maximum of 7.7-fold increase in luciferase activity was detected at a MOI ratio of 10/5.

This first set of data indicate that an optimal balance between the Tet R protein and the Tet O operator sequence integrated in cells is a key determinant to generate responsive cell lines to miRNA mimic used as inducer to switch OFF-to-ON the RILES configuration. Accordingly, the permissiveness of cells to lentivirus infection has to be taken into account when generating LentiRILES stable cell lines and might require optimized transduction procedures to bypass the low rate of viral infection of some cell lines (50).

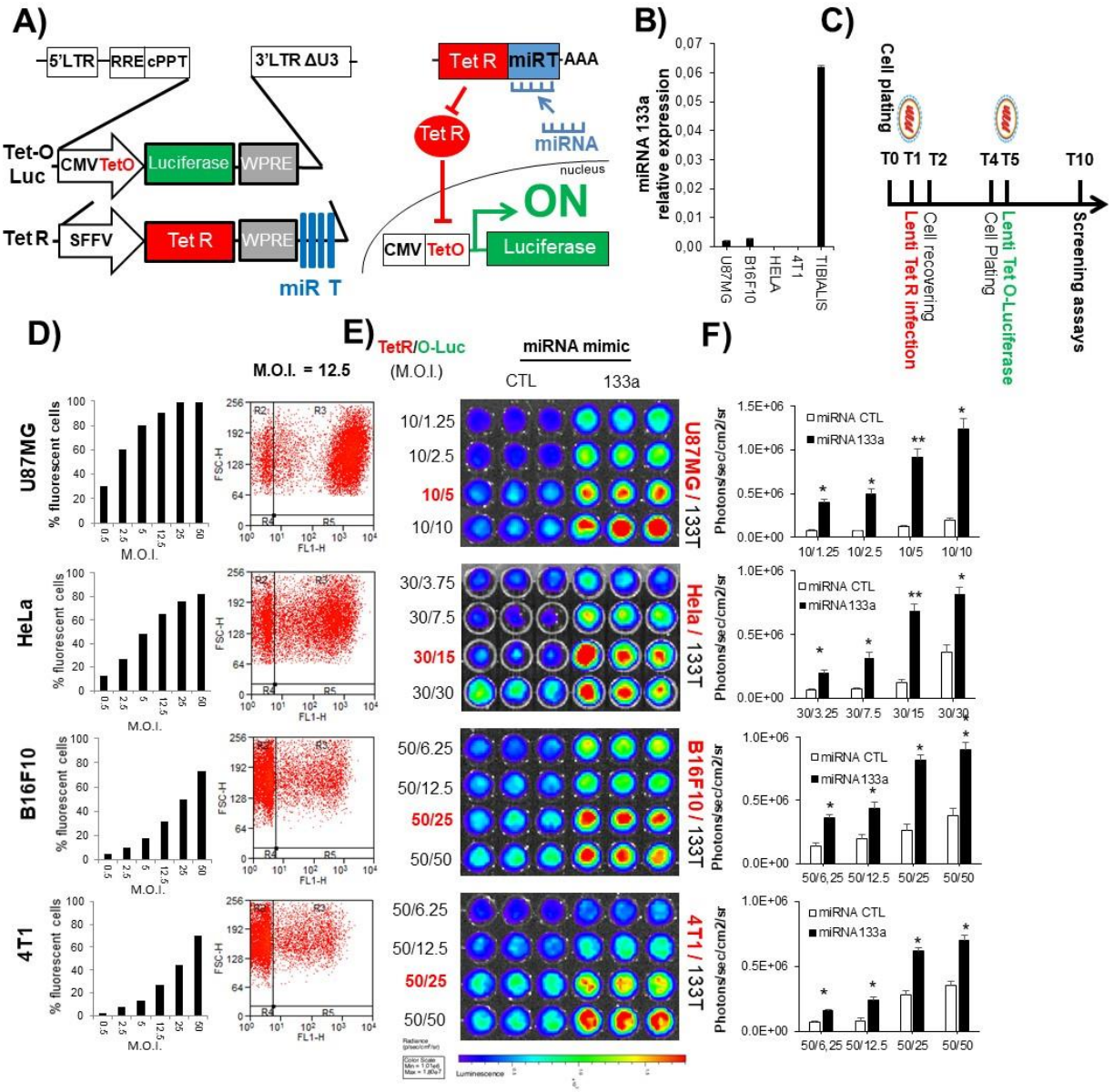

Figure 1. Schematic representation of the lentiRILES system and strategy to generate LentiRILES stable cell lines. **A)** Maps of the two lentiviral expression plasmids encoding for the RILES system. *Left panel*, Tet-O-Luc : lentivirus expression plasmid encoding for the firefly luciferase reporter gene driven by the inducible minimal CMV promoter containing 2 Tet O operators. Tet R : lentivirus expression plasmid encoding for the Tet R repressor protein controlled by the presence of a miRNA targeting sequence cassette (miR T) complementary to a miRNA sequence of interest. *Right panel*, Scheme showing luciferase induction upon miRNA activity. When expressed in cells, the miRNA of interest will bind to the miR T cassette located in the 3'UTR of the Tet R mRNA, inducing activation of the RISC machinery and transcriptional repression of the Tet R protein. In the absence of Tet R, the RNA polymerase transcribes the luciferase reporter gene, switching-ON the LentiRILES system. Bioluminescence signals emitted from the cells can be collected by bioluminescence imaging equipment. **B)** Quantitative RT-PCR analysis of miRNA-133a expression in several cancer cell lines and in the tibialis anterior skeletal muscles of mice used as positive control. **C)** Schematic representation of the procedure used to generate stable cell lines expressing the LentiRILES/133T system. The cells are first transduced with a constant MOI value of the Lenti Tet R/133T viral particles followed by the infection with different MOI values of lenti Tet-O-Luc viral particles to find the best balance between expression of the Tet R protein and the number of Tet O operators integrated in the host genome of cells. **D-F)** Production of different stable LentiRILES/133T cancer cell lines. **D**) Permissiveness of U87MG, Hela, B16F10 and 4T1 cells to lentivirus infection evaluated by flow cytometry using lentivirus particles encoding for the eGFP reporter gene at various MOI. **E**) Responsiveness to miRNA-133a of different U87MG, Hela, B16F10 and 4T1 cells LentiRILES/133T cell lines generated using different MOIs of TetR and Tet-O-Luc as indicated at the left of each lane of each wells of tissue culure plate. The LentiRILES/133T cell lines were plated on 24 well plates and then transfected with miRNA-133a before scanning the plate 3 days later using a bioluminescence imaging scanner. **F**). Quantitative bioluminescence signals collected from region of interest from E. Data are expressed as mean +/- SEM of one representative experiment performed at least 3 times. Statistics by the two-tailed t-test, *P<0.05, **P<0.01, compared to control cells transfected with a miRNA mimic control (CTL).

Characterization of the U87MG LentiRILES/133T Cell Line

We next performed a systematic analysis to gain insight into the molecular mechanism of the OFF-to-ON shift of the RILES/133T stably integrated in the genome of the LentiRILES U87MG/133T cell line (ratio 10/5). Results from qPCR analysis indicated that there were 2.1-times more viral integrated copies of Lenti TetR/133T than of Lenti_o_Luc virus in the host genome of these cells leading to to 64.1-fold higher relative production of Tet R mRNA in cells than Luciferase mRNA (Figure 2B and 2C). In the ON-configuration, *i.e*. after transfection of miRNA-133a, the relative expression of Tet R mRNA was reduced by 77.4 % (Figure 2B) corresponding to a reduction by 68.2 % of Tet R protein expression (Figure 2C). This downregulation process was correlated with the induction by 5.1-fold of the luciferase mRNA (Figure 2C) proving, as anticipated theoretically in Figure 1, that the mode

of shifting OFF-to-ON of the RILES system is dependent on the transcriptional repression of Tet R mRNA that, in turn, induces the expression of the Firefly Luciferase protein. We then evaluated the sensitivity of U87MG LentiRILES/133T cells. We found that the rate of luciferase fold induction was well correlated (R^2 = 0.97) with the concentration of miRNA-133a transfected in cells ranging from 0 to 3 nM (Figure 2E). However, above this concentration, the RILES read-out saturated. No statistically significant difference in terms of luciferase fold change was found between cells transfected with 3 nM and 100 nM of miRNA-133a (Figure 2E). The same trend was observed when the study was performed at the molecular level. The range of Tet R mRNA down-regulation was well correlated (R^2 = 0.92) with the increasing concentrations of miRNA-133a transfected in cells up to 3 nM, and was, as expected, inversely correlated (R^2 = 0.90) with the induction of luciferase reporter mRNA (Figure 2F). Again, above this miRNA concentration, the relative expression of both Tet R and luciferase mRNAs was not significantly different when 3 or 100 nM of miRNA-133a were transfected (figure 2F). We finally assayed the specificity of the LentiRILES/133T to several miRNA mimics transfected in cells. As shown in Figure 2G, no leakage or non-specific induction of the luciferase reporter gene was detected when irrelevant or unspecific miRNA mimics were used attesting again the great specificity of the RILES system (45-47).

This second set of data demonstrates that the LentiRILES system is a reliable, specific, sensitive OFF-to-ON shift miRNA-ON reporter system, capable to monitor the functionality of transfected miRNAs in several cancer cell lines. However, the saturation of RILES detected at intermediate concentrations of transfected miRNA mimics is perceptible and might be a limitation.

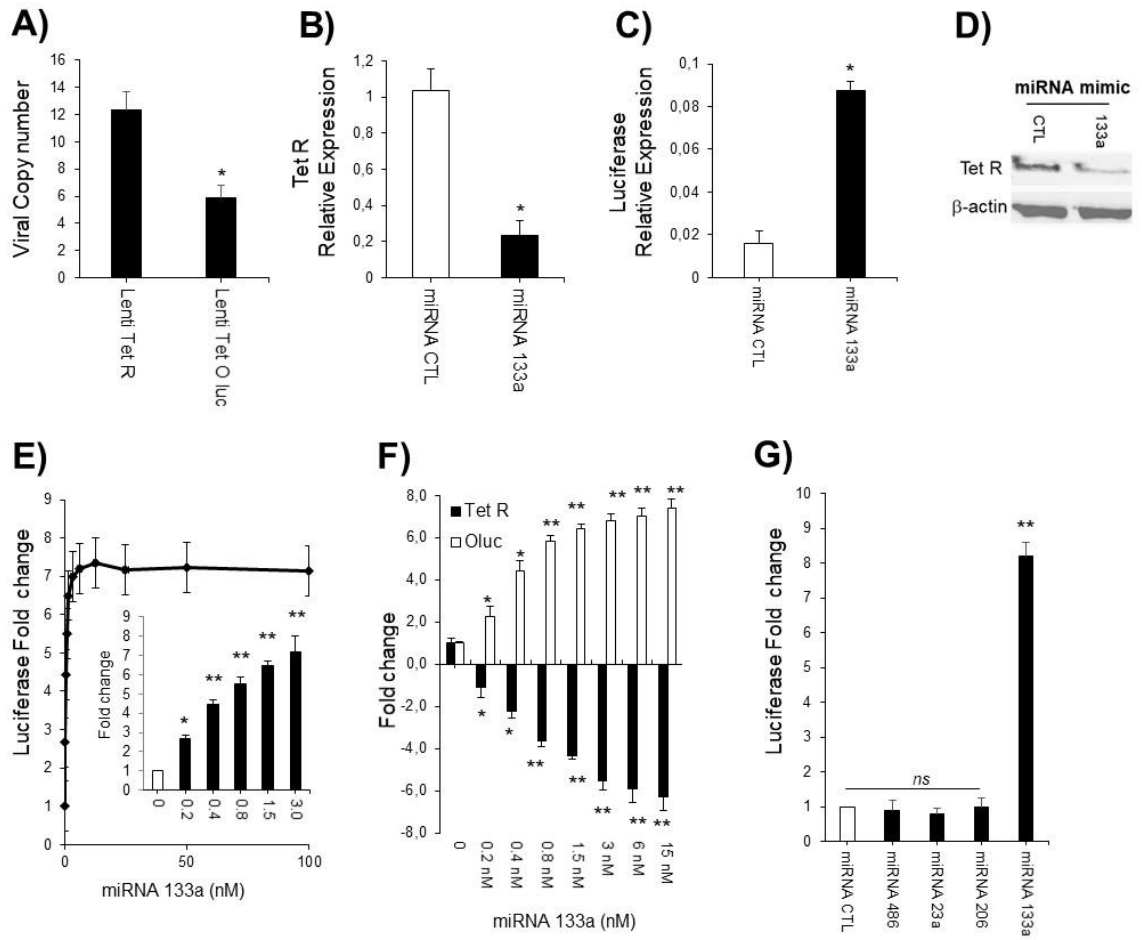

Figure 2. Functional characterization of the U87MG LentiRILES/133T cell line. **A)** Absolute quantitative PCR quantification to determine the number of viral copies of Lenti Tet R/133T and Lenti Tet-O-Luc expression plasmids integrated into the host genome of the U87MG LentiRILES/133T cell line. Relative Tet R (**B**) and luciferase (**C**) expression detected by quantitative RT-PCR in the U87MG LentiRILES/133T cell line before and after transfection of miRNA. **D)** Relative protein expression of Tet R protein detected by western blot in the U87MG LentiRILES/133T cell line before and after transfection of miRNA. **E)** Dose response study of luciferase fold change induction detected in the U87MG LentiRILES/133T cell line in response to increasing concentration of miRNA-133a mimic. Forty-eight hours after transfection, luciferase activity in cells was quantified and expressed as fold induction relative to control, not-transfected cells, and set to the arbitral value of 1. *Inset*: the same results but shown on a linear scale for miRNA concentration ranging from 0 to 3 nM. **F**) Relative Luciferase and Tet R fold change mRNA expression quantified by quantitative RT-PCR in U87MG LentiRILES/133T cells in response to increasing concentration of miRNA 133a. Data are expressed as mean +/- SEM of one representative experiments performed at least 3 times. Statistics by the two-tailed t-test, *P<0.05, **P<0.01, ns (not significant), compared to control cells transfected with a miRNA mimic control (CTL, B, C, G) or not-transfected cells (A, E, F).

In Vitro Monitoring of Endogenous Expressed Mirna Using the LentiRILES System

We then challenged a key aspect of miRNA biology that is related to the need for monitoring methods capable of resolving the dynamic expression pattern of endogenously expressed miRNAs during the development of physiological and pathological processes. We evaluated this challenging aspect using the two different cell types, C2C12 myoblast cells, that are known to express the miRNA-133a upon differentiation in myotubes (51) (Figure 3A) and U87MG cells that are known to have opposite expression patterns of miRNA-122 and -21.5p (52). To visualise the dynamic expression of these endogenously expressed miRNAs by fluorescence imaging on live cells, we replaced the Firefly Luciferase with the GFP reporter gene. The generated system was then denoted RIFES system, standing for RNAi-inducible fluorescence expression system.

C2C12 cells were transduced with an optimal Lenti Tet R/133T to Lenti Tet_O_eGFP MOI ratio according to the procedure described in Figure 1. Then the most responsive C2C12 LentiRIFES 133T stable cell line was differentiated in myotubes to induce expression of miRNA-133a (51). Fluorescence microscopy analysis of cell monolayers revealed presence of intense fluorescent signals in the differentiated myotubes formed, with stronger emitted fluorescence detected in areas where myotubes were more apparent (Figure 3C, arrows). In contrast, lower fluorescence signal was detected in undifferentiated, myoblast cell monolayers (Figure 3C) with a uniform distribution pattern of the fluorescence detected among the cellular monolayer. Quantitative flow cytometry analysis of the cells collected by trypsinization indicated that the mean GFP intensity was 3.9-fold higher in differentiated C2C12/133T myotubes compared to undifferentiated C2C12/133T myoblast cells (Figure 3D). Next, we monitored the endogenous expression pattern of miRNA-122 and -21.5p in U87MG cells which were found to be respectively faintly and highly expressed by qRT-PCR (Figure 3E). We constructed two novel LentiRIFES expression plasmids by replacing the 133T cassette with a 122T or 21.5T cassettes to produce the corresponding U87MG LentiRIFES/122T and -21.5T stable cell lines. We transfected these two cell lines with miRNA-122 mimic or with an inhibitor of miRNA-21.5 (AMO miRNA-21.5) (Figure 3F). Fluorescence microscopic analysis of cells monolayers in basal conditions revealed high fluorescence signal in the U87MG LentiRIFES/21.5T cells and low-to-almost undetectable fluorescence signal in the U87MG LentiRIFES/122T (Figure 3G) that correlated well with the endogenous expression pattern of these miRNAs detected by qRT-PCR (Figure 3E). Remarkably, a clear positive shift of fluorescence intensity, from 94 to 4 755 MFI was

quantified when the U87MG LentiRIFES/122T cells were transfected with miRNA-122 while, in contrast, a clear negative fluorescence shift from 7 547 to 3 231 MFI was detected when the U87MG LentiRIFES/21.5T cells were transfected with the miRNA-21.5 inhibitor.

This third set of data demonstrates that the LentiRILES system can not only monitor the expression of ectopic miRNA but also endogenously expressed miRNAs using two main optical molecular imaging modalities (*e.g* bioluminescent and fluorescent imaging). The fluorescent reporter gene offers an additional advantage for RILES by providing a single and live-cell resolution of miRNA expression that can be exploited to cell-sort homogenous populations of cells according to their miRNA expression pattern.

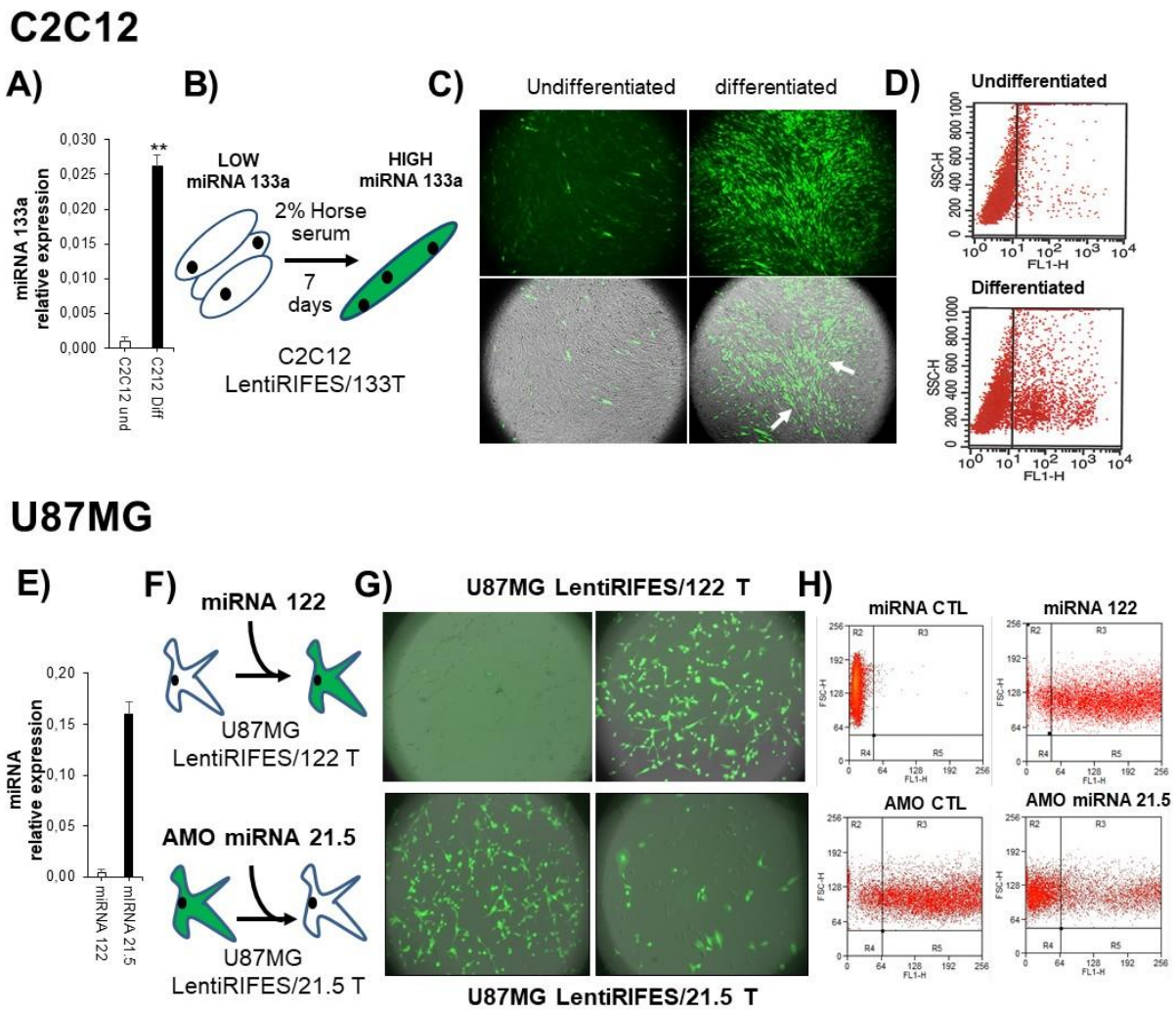

Figure 3. Real time, fluorescence monitoring of endogenously expressed miRNA in cell lines. **A**) Quantitative RT-PCR analysis of miRNA-133a expression in C2C12 cells cultured

in undifferentiated and differentiated media to induce differentiation of these cells in myotubes and the endogenous expression of miRNA-133a. **B)** Schematic representation of the procedure used to monitor expression of miRNA-133a in the myotubes using the RIFES/133T system and a fluorescence imaging microscope. The C2C12 cells were transduced with the Lenti Tet R/133T virus and then with Lenti_o_eGFF according to the procedure described in Figure 1C and then cultured in media containing 2% of horse serum to induce their differentiation in myotubes and expression of this miRNA. **C)** *Upper quadrant*, Live-cell fluorescence imaging of monolayers from undifferentiated and differentiated C2C12 LentiRIFES/133T cells performed at day 7. *Lower quadrant* superimposition of bright field and fluorescence images of the same field of view of cell monolayers to show the more pronounced localisation of fluorescence signals in the myotubes (arrows). **D)** Flow cytometry quantification of eGFP expression in the same cells as C collected by trypsinisation. **E)** Quantitative RT-PCR analysis of expression of miRNA-122 and -21.5 in U87MG cells. **F)** Schematic representation of the procedure to monitor expression of these two miRNAs in real-time by fluorescence imaging after transfection of miRNA-122 mimic or miRNA-21.5 inhibitor (AMO, antisense miRNA) in U87MG RIFES/122T and U87MG RIFES/21.5T cells respectively. **G)** Live-cell fluorescence imaging and **H)** flow cytometry analysis of the U87MG RIFES cells from F. Data are expressed as mean +/- SEM of one representative experiments performed at least 3 times. Statistics by the two-tailed t-test, **P<0.01 compared to control undifferentiated cells (C2C12 und).

The Lentiriles Cell Line can be used as a Positive Screening Platform to Identify Optimal Synthetic Mirna Mimics and Transfection Reagents

We next explored some applications of the LentiRILES system in the field of miRNA therapy. Having demonstrated the good sensitivity and specificity of the U87MG LentiRILES/133T cell line, we then anticipated that this cell line could be used as a novel, positive cell-based screening platform to evaluate the performance of miRNA mimics and transfection reagents. We screened the efficacy of 8 miRNA mimics and 7 transfection reagents commercially available. We included our homemade lipopolyplexes (LPRi) formulation, previously reported as a potent siRNA (53) and miRNA (47) transfection reagent as well as a synthetic homemade miRNA-133a mimic. Results of this screening procedure performed in 96-wells plate and monitored using a bioluminescence scanner indicated (Figure 5A) that the gold standard Lipofectamine RNAi max (7.24×10^{10} RLU/mg) and LPRi (6.82×10^{10} RLU/mg) transfection reagents were the two most efficient miRNA transfection reagents. The transfection reagent Transit X2 (4.93×10^{10} RLU/mg) and Hyperfect (4.63×10^{10} RLU/mg) exhibited a similar range of efficacy but were less efficient than the RNAi max and LPRi. The transfection reagents HappyFect (3.69×10^{10} RLU/mg), Viromer Blue (2.69×10^{10} RLU/mg), Fugene HD (2.63×10^{10} RLU/mg) and Fugene 6 (2.46×10^{10} RLU/mg) were found the less efficient (Figure 4A, lower panel). Using a similar

approach (Figure 5B), we found that the best miRNA mimic tested was the miRVANA mimic from ThermoFisher (7.59 x 10^{10} RLU/mg) followed closely by the mimic produced by Qiagen (6.89 x 10^{10} RLU/mg). The miRNA mimics produced by Dharmacon (4.83 x 10^{10} RLU/mg), Active Motif (4.66 x 10^{10} RLU/mg), by our laboratory (HM, 4.43 10^{9} RLU/) and by Sigma (4.03 x 10^{10} RLU/mg) were less efficient. We also found that the first generation of miRNA mimic produced by ThermoFisher, called pre-miRNA, was less efficient (3.93 x 10^{10} RLU/mg) than miRVANA (7.24 x 10^{10} RLU/mg) which is the latest generation of miRNA mimics produced by the company. According to this company, the difference between these two generations of synthetic miRNAs can be attributed to proprietary-based chemical modifications of miRNA oligonucleotides. It is therefore interesting to point out that the LentiRILES monitoring system is sensitive enough to discriminate by an almost 2-fold difference in sensitivity between these two generations of miRNA mimics.

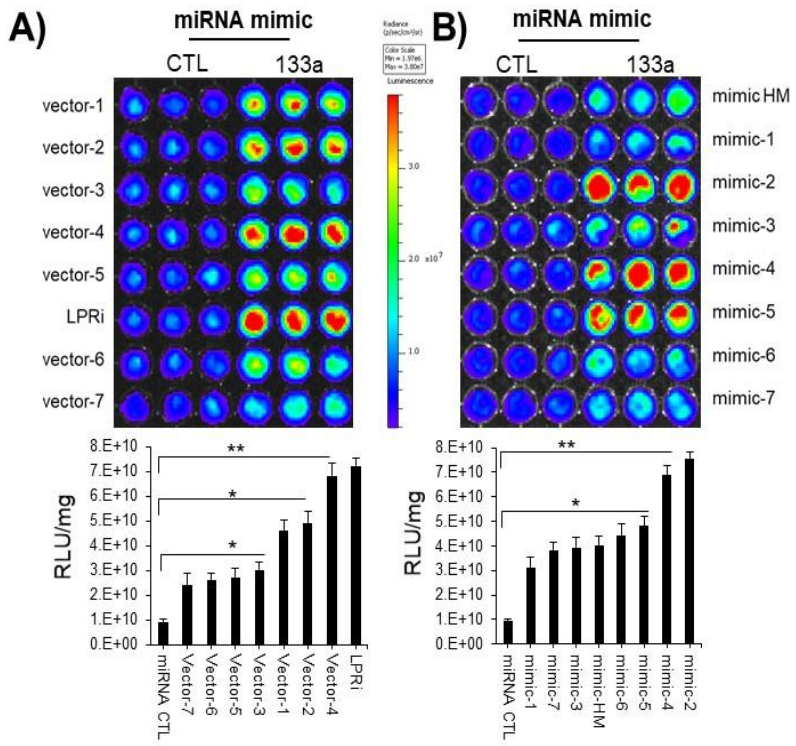

Figure 4. Cell-based miRNA screening platform using the U87MG LentiRILES/133T cell line. The U87MG LentiRILES/133T cells were plated on 96-well plates and then transfected with commercially available **A)** transfection reagents and **B)** miRNA-133a mimics. A homemade miRNA-133 mimic (mimic HM) and lipopolyplexes transfection reagent (LPRi) were included. *Upper panel* : the plates were scanned 3 days later using a bioluminescence scanner. *Lower panel* : same experiment performed on 24-wells plate to normalize bioluminescence values to protein contents in each wells. The data were expressed as mean of RLU/mg +/- SEM of one representative experiment performed at least 3 times. Statistics

by the two-tailed t-test, *P<0.05, **P<0.01, compared to control cells transfected with a miRNA mimic control (miRNA CTL).

We then examined another possible application of our LentiRILES system by exploring some key features of the relationship between the structure and function of miRNA duplexes (54-56). We prepared two types of miRNA-133a mimic (Figure 5A): a blunt-end extremity of miRNA-133a duplex and a 3' dinucleotide overhang miRNA-133a duplex identical to the double-stranded miRNA-133a duplex produced endogenously by the cells and annotated in the mirBAse data base. As impact of the miRNA structures on their intracellular fate in cells after transfection was not reported to our knowledge, we first investigated whether the change in the miRNA structure duplex from asymmetric 3'overhang structure to symmetric blunt structure would affect their intracellular distribution as well as their co-localization with the Argonaute 2 protein. Confocal fluorescence microscopy analysis in Figure 5B demonstrated that the intracellular distribution of the two miRNA structures labelled with Cyanine 3 was similar and also equally co-localized with the Argonaute 2 protein as revealed by immunofluorescence labelling. The determination of the Pearson coefficient (PC) index confirmed this observation as no statistically significant difference was found between the co-localization indices of Argonaute 2 with the overhang (PC = 0.225) and blunt (PC = 0.232) miRNA duplexes (Figure 5C). In contrast, the functionality of these 2 miRNA duplexes were different (Figure 5D). The overhang, asymmetric miRNA-133a duplex activated by 4.2-fold the RILES/133T system while the symmetric miRNA-133a duplex activated by only 2.4-fold. This demonstrates that the RISC machinery preferentially processed the overhang, asymmetric miRNA-133a duplex rather than the blunt, symmetric miRNA-133a duplex. These results are in line with previous studies indicating that 3' nucleotide overhang asymmetric duplex miRNA is a key structural parameter that governs the incorporation and selection of one strand from the miRNA duplex by the RISC machinery, a phenomenon referred to as the thermodynamic asymmetry rule of RNAi duplex (57). We therefore anticipated that the blunt-end miRNA duplex does not favour such a selection and thus that the RISC machinery might process equally the two strands of miRNA duplexes. The lower luciferase induction monitored by RILES with the blunt-end miRNA duplex can be explained by a direct competition of the two strands of the miRNA-133a duplex for binding to the miR-133T cassette in cells which is specific to the mature strand sequence of miRNA 133, not the passenger strand.

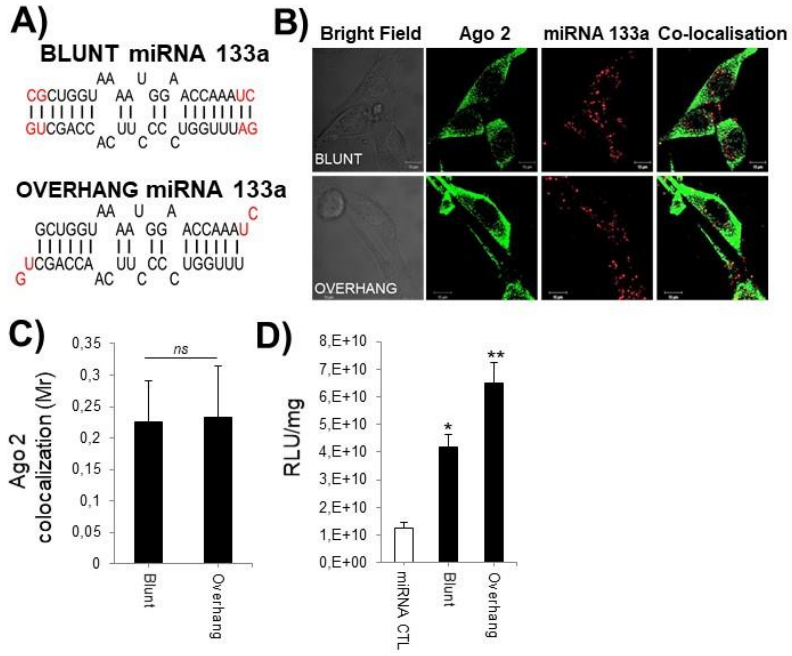

Figure 5. Structure and function relationship study of miRNA-133a duplexes using the U87MG LentiRILES/133T cell line. **A**) Schematic representation of the structure of the two synthetic miRNA-133a duplexes produced in our laboratory that harbour either blunt-end or 3' dinucleotide overhang extremities. **B**) Confocal microscopy analysis of U87MG cells transfected with Cy3-labelled miRNA-133a from A. **C**) Percentage of co-localization of Cy3-labelled miRNA-133a from B with Argonaute 2 protein revealed by immunofluorescence staining. **D**) Luciferase activities normalized to protein content (RLU/mg) from U87MG LentiRILES/133T cells transfected with miRNA-133a from A. Data are expressed as mean +/- SEM of representative experiments performed at least 3 times. Statistics by the two-tailed t-test, *P<0.05; **P<0.01, compared to control cells transfected with a miRNA mimic control (miRNA CTL).

In Vivo Bioluminescence Monitoring of the Kinetic of Mirna Activity Upon Delivery in an Orthotopic Animal Model of Glioblastoma.

A key aspect that has not yet been fully achieved in the field of miRNA therapeutics is the ability to resolve the kinetic of miRNA functionality once delivered in the tumour mass. Better understanding of the long-term activity of synthetic miRNA mimics or inhibitors in targeted tissues would be an advantage to optimize an administration protocol to deliver maximal dose of therapeutic miRNA with minimal toxicity (58, 59). This point is particularly of interest when considering the locoregional treatment of tumour mass located in vulnerable organs such as the brain furthermore isolated from the rest of the body by the blood brain barrier. Recent advances into clinical practice indicated that the convection-enhanced delivery method is a reliable approach to deliver high drug content in specific areas of the

brain, bypassing as such the blood brain barrier that prevents therapeutic drugs from reaching the central nervous system. The principle of this delivery method consists in applying a constant pressure gradient to an infusion tip in such way that the fluid flow driven by the convection force allows the drugs to diffuse over large distance and period of time (49, 60-62). However, as this locoregional procedure can be considered as invasive, optimal administration procedures are required to limit the repetition of surgical intervention to implant catheters into the brain without compromising the therapeutic outcome.

Using bioluminescence imaging, we attempted to resolve the dynamics of miRNA activity upon delivery in glioblastoma tumour mass by CED. We implanted the U87MG LentiRILES/133T cells into the striatum of SCID mice. Ten days later the developed tumour mass were infused with the miRNA-133a complexed with our LPRi nanocarrier by CED (Figure 6A). The mice were thereafter scanned using a bioluminescence imaging scanner over a longitudinal study of 2 weeks (Figure 6B). Typical bioluminescence images collected at several time points from one illustrative mouse per group are shown in Figure 6C.

Bioluminescence analysis of each mice followed over time revealed that the basal luciferase activity of RILES detected in the LPRi_miRNA control group of mice increased proportionally with the tumour proliferation over time (Figure 6B, left panel). In contrast, upon CED infusion of miRNA-133a and thus switching lentiRILES in the ON-configuration, a different pattern of luciferase activity was detected in the LPRi_miRNA-133a group of mice (Figure 6B, right panel). Three of the five mice exhibited two peaks of luciferase activity detected either at day 4 (mouse 546) or day 6 (mice 550 and 549), indicating that the delivery of miRNA-133a mimic was successful in these 3 tumours but also variable. As shown in the right panel of Figure 6B, the luciferase fold change values monitored in mouse #550 and #549 increased gradually over time, reached a maximum peak of activity at day 6 and then dropped, two days later, to the basal level, similar to that detected in the control group (LPRi_miRNA CTL mice, Figure 6B). In contrast, the luciferase activity monitored in mice #546 increased more rapidly in the first 4 days, reached a maximum at this time point (*e.g* day 4) and decreased quickly thereafter to finally reaching the basal bioluminescence levels detected in the control group.

The factors contributing to the heterogeneity of miRNA delivery observed by RILES in these mice are currently not clear and several hypothesis can be inferred. The interaction with

the extracellular matrix might allow the LPRi_miRNA-133a nanoparticles to be gradually released in the tumour microenvironment, thus serving as extra-cellular reservoirs (63). Physical parameters, such as pH values, salt concentration, interstitial tumour fluid pressure can also impact the release rate of LPRi_miRNA-133a nanocarriers from infusion tips into the solid tumours (64-67). Tumour cells intrinsic processing or recycling of transfected miRNAs through extracellular vesicles can also be involved (68, 69) resulting in a long-lasting activity of transfected miRNAs in solid tumour as we recently reported in U87MG cells (47). While deciphering the exact mechanism of miRNAs diffusion into the brain was not the scope of this study, future experiments are planned to elucidate this process. This study is the first to our knowledge that reports in real time and as a positive readout the kinetic of miRNA delivery and activity in a preclinical animal model of brain tumour.

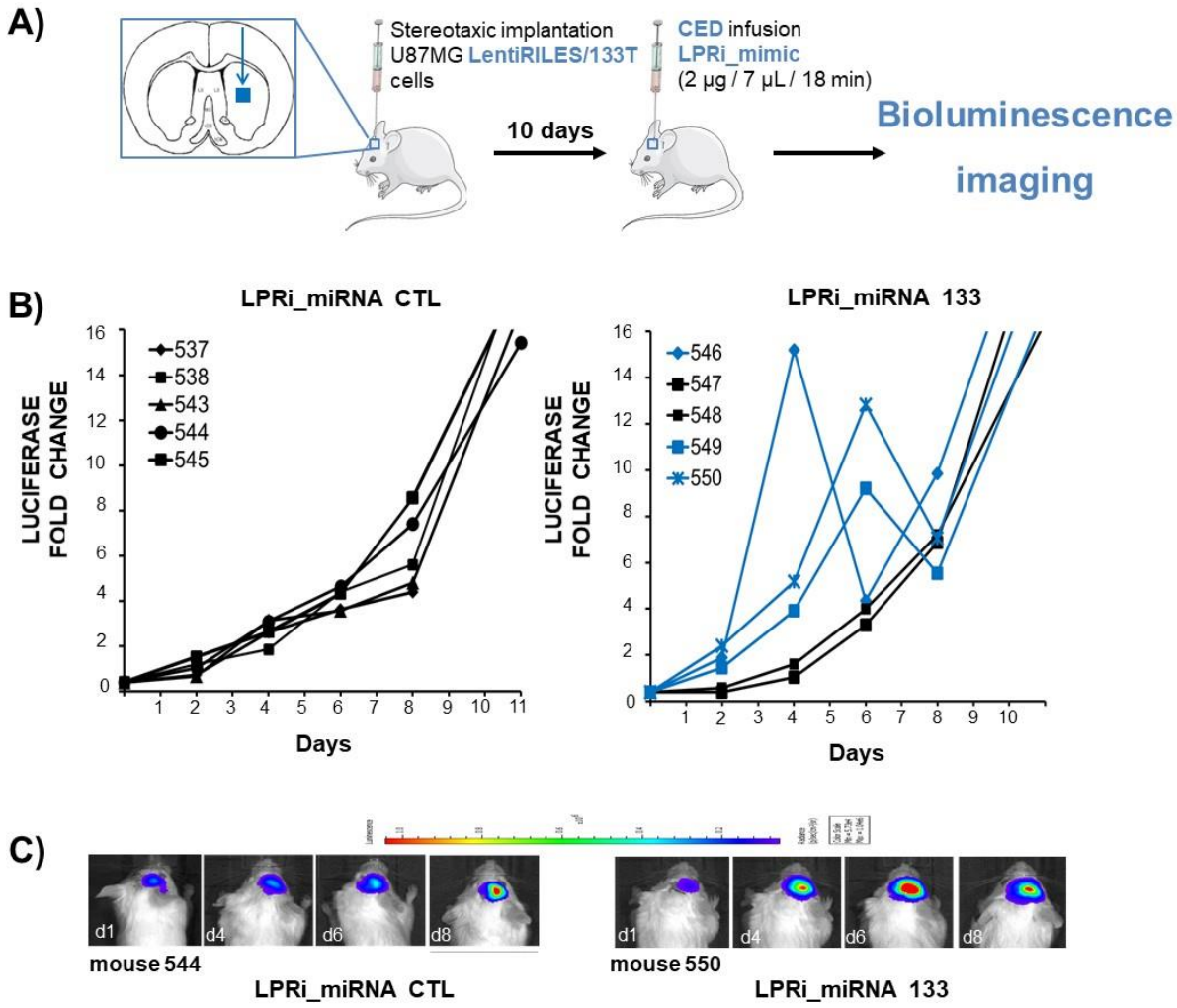

Figure 6. *In vivo* bioluminescence monitoring of kinetic of miRNA-133a activity upon delivery in an orthotopic glioblastoma mouse model. **A**) Schematic representation of the

procedure used to establish the kinetic of miRNA-133a *in vivo*. The U87MG LentiRILES/133T cells were implanted in the striatum of mice by stereotaxic surgery and then, 10 days later when the mice developed solid tumours, the miRNA-133a or miRNA control (CTL) were formulated with the LPRi lipopolyplexes and infused locally in tumour masses by convection-enhanced delivery. **B**) Quantitative bioluminescence signals emitted from the brain of mice infused with the LPRi_miRNA-133a and LPRi_miRNA CTL and collected in real time using an *in vivo* bioluminescence scanner. Data are expressed as luciferase activity fold change by normalizing bioluminescence values detected for each mouse at the indicated time point to the minimal value detected on the day of infusion and set to the arbitral value of 1. **C**) Representative bioluminescence images collected from one representative mouse from the LPRi_miRNA-133a and LPRi_miRNA CTL group of animals.

Therapeutic Evaluation of Mirna-200c in the Orthotopic Animal Model of Glioblastoma

Finally, we decided to evaluate the therapeutic relevancy of a locoregional RNAi treatment of glioblastoma by infusion of tumour beds with a tumour suppressor miRNA by CED guided by the RILES (Figure 6). Over the last decade, a growing number of tumour suppressor miRNAs have been discovered to play pivotal roles in tumorigenesis (70, 71). We decided to focus our experiments on the tumour suppressor miRNA-200c (72, 73). Gain-of-function studies performed in our laboratory indicated that transfection of miRNA-200c in U87MG cells impaired significantly the proliferation rate of these tumour cells (Figure 7A) by inducing cell cycle arrest in G1 phase (Figure 7B) but without inducing apoptosis (Figure 7C). We observed a drastic change in the morphology of U87MG cells after miRNA-200c transfection (data not shown) and investigated whether the ectopic expression miRNA-200c in these cells might induce a reversal phenotype from the mesenchymal to the epithelial phenotype (MET). As shown in Figure 7D, significant reduction of relative mRNAs expression of mesenchymal markers, ZEB-1 (38.2 % reduction), ZEB-2 (49.4 % reduction) and Vimentin (21 % reduction) were detected after miRNA-200c transfection, which correlated with the *de novo* expression of epithelial E-Cadherin marker(16.3-fold increase). Based on this data, we evaluated the impact of this change in the cell morphology on the migratory behaviour of the U87MG cells. Wound-healing scratch assay in Figure 7E demonstrated that transfection of miRNA-200c significantly delayed ($p = 0.028$) the migratory capability of the U87MG cells, notably at the 22 hours time point where the percentage of wound closure was reduced by 51.3 %. Overall, these biological changes in U87MG cells are relevant for glioblastoma treatment as this tumour type is characterized by rapid growth and local invasion of surrounding tissue (74-76). Furthermore, Quin et al. (77) demonstrated that the stable overexpression of miRNA-200c in glioblastoma reduced the

proliferation and invasion rate of glioma cells *in vitro* and *in vivo* in a subcutaneous xenografts animal model of glioblastoma. Although this study has merit as it provides novel insights into the mode of action of miRNA-200c in a glioblastoma context, it cannot objectively, as acknowledged by the authors, inquire into the therapeutic value of miRNA-200c to treat brain tumours.

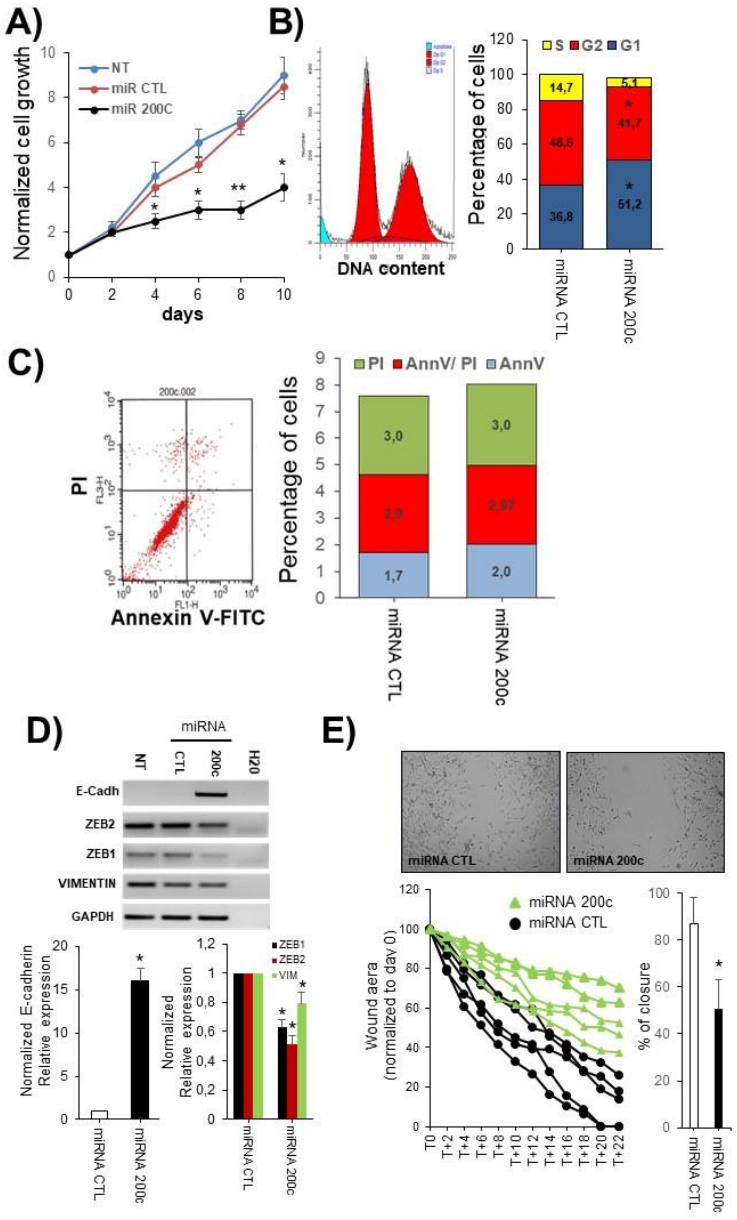

Figure 7. Tumour suppressive function evaluation of miRNA-200c in U87MG cells *in vitro*. **A**) Alamar Blue cell proliferation assay, **B**) flow cytometry analysis of cell cycle and **C**) apoptosis assay of U87MG cells transfected with miRNA-200c or miRNA control (miRNA CTL). **D**) *Upper panel:* Agarose gel analysis of the RT-PCR products generated with specific primers to detect expression of the E-cadherin, vimentin, ZEB1 and ZEB2 EMT markers after transfection of U87MG cells with miRNA-200c or miRNA control (miRNA CTL). *Lower panel*: the same experiment analysed by quantitative RT-PCR. **E)** Wound

healing assay of U87MG cells transfected with miRNA-200c or miRNA control (miRNA CTL). *Upper panel*, representative pictures of cell monolayers collected 16 hours after wound scratch. *Lower panel*, *left*, time lapse of wound area closure measured by imaging software from pictures taken every 2 hours over a period of time of 24 hours. *Lower panel*, *right,* percentage of wound closure from U87MG cell transfected with miRNA-200c or miRNA control (miRNA CTL) normalized to the wound surface area detected at T0 and set to the arbitral value of 1. Data are expressed as mean +/- SEM of one representative experiments performed at least 3 times. Statistics by the two-tailed t-test, *P<0.05, **P<0.01, compared to control cells transfected with miRNA mimic control (miRNA CTL).

We decided to address this point using a miRNA delivery approach to closely mimic a clinical intervention in which the miRNA-200c will be infused directly into the tumour mass using a miRNA-nanocarrier, the LPRi lipopolyplexes and the CED as delivery method. As the RILES system indicated that the delivered miRNAs are active for 4 to 6 days upon delivery (Figure 6), we infused the U87MG solid tumours twice with the LPRi_miRNA-200c by CED, spaced by an interval of time of 4 days (Figure 8A). The therapeutic impact of this targeted miRNA-200c delivery approach in glioblastoma development was evaluated by magnetic resonance imaging (MRI) performed over a 3 weeks period of time.

As shown in Figure 8B, the overall growth rate of tumour development was found similar between the LPRi_miRNA CTL and LPRi_miRNA-200c group of animals although a plateau of growth of tumour mass was visible between days 11 to 14 in the LPRi_miRNA-200c group of animals. Statistical analysis performed at day 14 indicated that tumour volumes in the LPRi_miRNA-200c group of animals were significantly smaller ($p = 0.03$, Figure 8C) than those detected in the LPR_miRNA CTL group of animals. Representative MRI of one representative tumour mass by group of animal is showed in Figure 8D. Smaller size of tumour mass is noticeably visible at this time point. However, beyond this time frame no other statistically significant difference was found. These results indicate that the treatment of glioblastoma tumours twice with the LPRi_miRNA-200c can significantly delay the proliferation rate of tumour cells but this effect is transient and reversible. The Kaplan Meier survival curves draw from this experience confirm the above statement. Although the median survival time of the two groups of animals differed by 2 days in beneficial of the miRNA-200c group of animals, no statistically significant difference was observed between these two groups of animals (Figure 8E).

Based on this data, it might be tempting to speculate that repeated administrations (*i.e*. more than twice) of the LPRi_miRNA-200c might be necessary to reach a better therapeutic outcome. However, as we observed *in vitro* that miRNA-200c exerted a mild cytostatic effect in U87MG tumour cells, characterized by a cell cycle arrest of U87MG cells in G1 and S-phase without inducing apoptosis (Figure 7 A-C), locoregional therapeutic intervention of glioblastoma with miRNA-200c mimic needs to be addressed with caution. A combinatorial treatment with another therapeutic agent might be required to reach a better curative treatment. In the specific context of glioblastoma, a combined treatment of miRNA-200c with radiotherapy seems particularly suitable. External beam therapy has long been used as a keystone treatment in glioblastoma patients but results from clinical studies indicated that combinatory treatments are required for an optimal therapeutic outcome (78). Interestingly, it was recently reported that overexpression of miRNA-200c in different cancer cells including glioblastoma inhibited invasion, migration, and vascular tube formation and increased the radiosensitivity of tumour cells by modulating the EGFR signalling pathway and favouring persistence of the γH2AX focus (79). Exploiting the radio-sensitizing properties of miRNA-200c in combination with a radiotherapy protocol deserves to be addressed *in vivo*. Repeated administration of miRNA-200c, guided by RILES after radiotherapy, might provide a therapeutic advantage. We are currently assaying this point as well as investigating the radiosensitizing role of other miRNA candidates recently identified through a molecular screening procedure applied on biopsies of patients with radioresistant glioblastoma tumours.

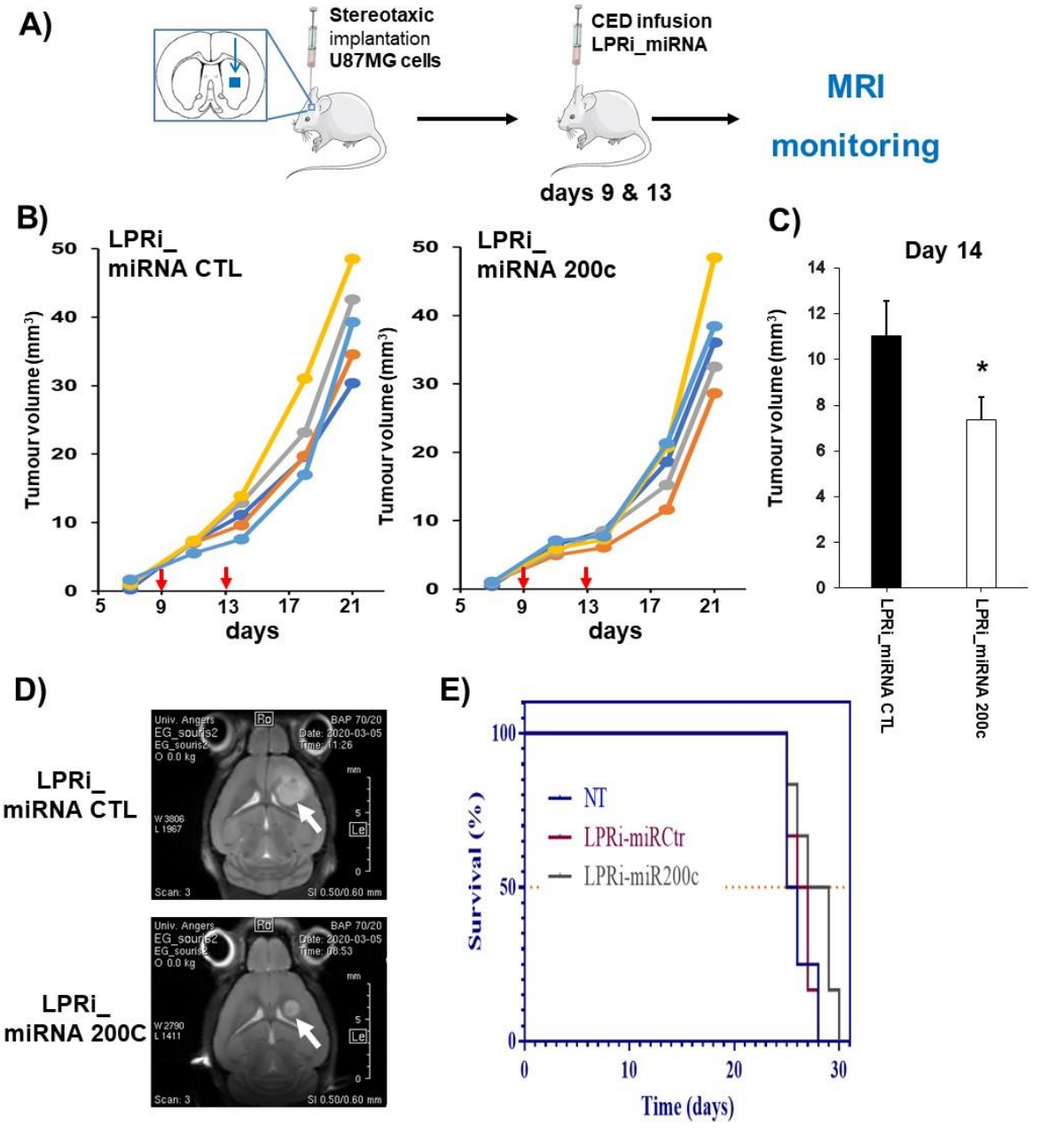

Figure 8. Tumour suppressive evaluation of miRNA-200c in a preclinical animal model of glioblastoma. **A**) Schematic representation of the procedure used to evaluate the therapeutic potential of miRNA-200c. The U87MG cells were implanted in the brain of mice and then when the mice developed solid tumours, the miRNA-200c or miRNA control were formulated with the LPRi lipopolyplexes and infused locoregionally, twice, at days 9 and 13 by convection-enhanced delivery. **B**) Tumour growth in both treatment groups monitored by MRI imaging once a week. **C**) Statistical analysis of tumour volumes collected at day 14 from the two groups of animals (n = 5 for each). **D**) Representative MRI performed at day 14 after implantation of U87MG cells (arrows indicate tumour tissue). **E**) Kaplan Meier curve. Data are expressed as mean +/- SEM of one representative experiment performed twice. Statistics by the two-tailed t-test, *P<0.05 compared to control group of animal infused with the LPRi_miRNA CTL.

Conclusion

Taken together, our work demonstrates that the genetic-switch RILES expression system integrated in a lentivirus is a relevant approach to monitor the endogenous and exogenous dynamic expression of miRNAs in fast-dividing biology systems such as cancer cells. We performed a complete set of validation studies at the molecular and cellular level and demonstrated that LentiRILES is a robust, specific and sensitive integrative miR-ON monitoring system that can be exploited to resolve the dynamic of miRNA activity over short (47) and, here, long periods of time. We explored several applications of LentiRILES in the field of miRNA biology and therapeutics *in vitro* and demonstrated the feasibility of this novel system for *in vivo* monitoring of miRNA mimic delivery. Because of its relatively easy production and versatility, we anticipate that the LentiRILES system holds promise for multiple applications in the field of miRNA biology as well as gene and cellular therapy.

Acknowledgement

We thank Stéphanie Lerondel, Maryline Le Mée, Stéphanie Rétif and Julien Sobilo (TAAM/CIPA, CNRS UPS 44, Orléans) for their technical assistance and for access to the Lumina Bioluminescence scanner. We also thank Elizabeth Rowley-Jolivet (elizabeth.rowley-jolivet@orange.fr) for English language editing.

Funding

This work was funded by the Institut National du Cancer (INCa) [PL-BIO 2014–2020, consortium MARENGO : MicroRNA agonist and antagonist Nanomedicines for GliOblastoma treatment: from molecular programming to preclinical validation to P.B and E.G]; La Ligue Contre le Cancer [Région du Loiret 2017-2019 to P.B]; ARD 2020 Biopharmaceuticals [RNA cell factory 2017-2020 to C.P]. The work was also related to the French National Research Agency (ANR) through the LabEx IRON (Innovative Radiopharmaceuticals in Oncology and Neurology) as part of the French government Investissements d'Avenir program (ANR-11-LABX-0018) and to the ANR under the frame

of EuroNanoMed III (project GLIOSILK). LR was a PhD fellow funded by the LabEx IRON-2 and the University of Angers.

Competing interests

Francisco Martin is inventor of "Highly inducible dual-promoter lentiviral Tet-On" (CT/EP2012/059408) licensed to Canvax Biotech.

References

1. Nazarov PV, Reinsbach SE, Muller A, Nicot N, Philippidou D, Vallar L, et al. Interplay of microRNAs, transcription factors and target genes: linking dynamic expression changes to function. Nucleic acids research. 2013;41(5):2817-31. PMCID: 3597666.
2. O'Brien J, Hayder H, Zayed Y, Peng C. Overview of MicroRNA Biogenesis, Mechanisms of Actions, and Circulation. Front Endocrinol (Lausanne). 2018;9:402. PMCID: 6085463.
3. Osada H, Takahashi T. MicroRNAs in biological processes and carcinogenesis. Carcinogenesis. 2007;28(1):2-12.
4. Cai X, Hagedorn CH, Cullen BR. Human microRNAs are processed from capped, polyadenylated transcripts that can also function as mRNAs. RNA. 2004;10(12):1957-66. PMCID: 1370684.
5. Lee Y, Ahn C, Han J, Choi H, Kim J, Yim J, et al. The nuclear RNase III Drosha initiates microRNA processing. Nature. 2003;425(6956):415-9.
6. Grishok A, Pasquinelli AE, Conte D, Li N, Parrish S, Ha I, et al. Genes and mechanisms related to RNA interference regulate expression of the small temporal RNAs that control C. elegans developmental timing. Cell. 2001;106(1):23-34.
7. Hutvagner G, McLachlan J, Pasquinelli AE, Balint E, Tuschl T, Zamore PD. A cellular function for the RNA-interference enzyme Dicer in the maturation of the let-7 small temporal RNA. Science. 2001;293(5531):834-8.
8. Jonas S, Izaurralde E. Towards a molecular understanding of microRNA-mediated gene silencing. Nature reviews Genetics. 2015;16(7):421-33.
9. Wu J, Yang J, Cho WC, Zheng Y. Argonaute proteins: Structural features, functions and emerging roles. J Adv Res. 2020;24:317-24. PMCID: 7235612.
10. Gebert LFR, MacRae IJ. Regulation of microRNA function in animals. Nature reviews Molecular cell biology. 2019;20(1):21-37. PMCID: 6546304.
11. Huntzinger E, Izaurralde E. Gene silencing by microRNAs: contributions of translational repression and mRNA decay. Nature reviews Genetics. 2011;12(2):99-110.
12. Shivdasani RA. MicroRNAs: regulators of gene expression and cell differentiation. Blood. 2006;108(12):3646-53. PMCID: 1895474.
13. Rupaimoole R, Slack FJ. MicroRNA therapeutics: towards a new era for the management of cancer and other diseases. Nature reviews Drug discovery. 2017;16(3):203-22.
14. Lim LP, Lau NC, Weinstein EG, Abdelhakim A, Yekta S, Rhoades MW, et al. The microRNAs of Caenorhabditis elegans. Genes & development. 2003;17(8):991-1008. PMCID: 196042.
15. Sokol NS. Small temporal RNAs in animal development. Curr Opin Genet Dev. 2012;22(4):368-73. PMCID: 3419770.

16. Pauli A, Rinn JL, Schier AF. Non-coding RNAs as regulators of embryogenesis. Nature reviews Genetics. 2011;12(2):136-49. PMCID: 4081495.
17. Ebert MS, Sharp PA. Roles for microRNAs in conferring robustness to biological processes. Cell. 2012;149(3):515-24. PMCID: 3351105.
18. Wightman B, Ha I, Ruvkun G. Posttranscriptional regulation of the heterochronic gene lin-14 by lin-4 mediates temporal pattern formation in C. elegans. Cell. 1993;75(5):855-62.
19. Reinhart BJ, Slack FJ, Basson M, Pasquinelli AE, Bettinger JC, Rougvie AE, et al. The 21-nucleotide let-7 RNA regulates developmental timing in Caenorhabditis elegans. Nature. 2000;403(6772):901-6.
20. Johnson SM, Lin SY, Slack FJ. The time of appearance of the C. elegans let-7 microRNA is transcriptionally controlled utilizing a temporal regulatory element in its promoter. Dev Biol. 2003;259(2):364-79.
21. Bracht JR, Van Wynsberghe PM, Mondol V, Pasquinelli AE. Regulation of lin-4 miRNA expression, organismal growth and development by a conserved RNA binding protein in C. elegans. Dev Biol. 2010;348(2):210-21. PMCID: 2982876.
22. Kai ZS, Finnegan EF, Huang S, Pasquinelli AE. Multiple cis-elements and trans-acting factors regulate dynamic spatio-temporal transcription of let-7 in Caenorhabditis elegans. Dev Biol. 2013;374(1):223-33. PMCID: 3548979.
23. Kucherenko MM, Barth J, Fiala A, Shcherbata HR. Steroid-induced microRNA let-7 acts as a spatio-temporal code for neuronal cell fate in the developing Drosophila brain. EMBO J. 2012;31(24):4511-23. PMCID: 3545287.
24. Li T, Pan H, Li R. The dual regulatory role of miR-204 in cancer. Tumour Biol. 2016;37(9):11667-77. PMCID: 5080331.
25. Jiang H, Zhang G, Wu JH, Jiang CP. Diverse roles of miR-29 in cancer (review). Oncol Rep. 2014;31(4):1509-16.
26. Dykxhoorn DM. MicroRNAs and metastasis: little RNAs go a long way. Cancer Res. 2010;70(16):6401-6. PMCID: 2922433.
27. Ma L. Role of miR-10b in breast cancer metastasis. Breast Cancer Res. 2010;12(5):210. PMCID: 3096969.
28. Lee SJ, Kim MJ, Kwon IC, Roberts TM. Delivery strategies and potential targets for siRNA in major cancer types. Advanced drug delivery reviews. 2016;104:2-15. PMCID: 4958528.
29. Jones D. Setbacks shadow microRNA therapies in the clinic. Nat Biotechnol. 2018;36(10):909-10.
30. Setten RL, Rossi JJ, Han SP. The current state and future directions of RNAi-based therapeutics. Nature reviews Drug discovery. 2019;18(6):421-46.
31. Kang WJ, Cho YL, Chae JR, Lee JD, Choi KJ, Kim S. Molecular beacon-based bioimaging of multiple microRNAs during myogenesis. Biomaterials. 2011;32(7):1915-22.
32. Hernandez R, Orbay H, Cai W. Molecular imaging strategies for in vivo tracking of microRNAs: a comprehensive review. Curr Med Chem. 2013;20(29):3594-603. PMCID: 3749288.
33. Baker MB, Bao G, Searles CD. In vitro quantification of specific microRNA using molecular beacons. Nucleic acids research. 2012;40(2):e13. PMCID: 3258119.
34. Schug J, McKenna LB, Walton G, Hand N, Mukherjee S, Essuman K, et al. Dynamic recruitment of microRNAs to their mRNA targets in the regenerating liver. BMC Genomics. 2013;14:264. PMCID: 3639193.
35. Kim HJ, Kim YH, Lee DS, Chung JK, Kim S. In vivo imaging of functional targeting of miR-221 in papillary thyroid carcinoma. J Nucl Med. 2008;49(10):1686-93.
36. Pichard V, Aubert D, Boni S, Battaglia S, Ivacik D, Nguyen TH, et al. Specific micro RNA-regulated TetR-KRAB transcriptional control of transgene expression in viral vector-transduced cells. PloS one. 2012;7(12):e51952. PMCID: 3522580.

37. Amendola M, Giustacchini A, Gentner B, Naldini L. A double-switch vector system positively regulates transgene expression by endogenous microRNA expression (miR-ON vector). Molecular therapy : the journal of the American Society of Gene Therapy. 2013;21(5):934-46. PMCID: 3666624.
38. Rossetti S, Anauo MJ, Sacchi N. MiR-221-regulated KIT level by wild type or leukemia mutant RUNX1: a determinant of single myeloblast fate decisions that - collectively - drives or hinders granulopoiesis. Oncotarget. 2017;8(49):85783-93. PMCID: 5689646.
39. Ecco G, Imbeault M, Trono D. KRAB zinc finger proteins. Development. 2017;144(15):2719-29.
40. Rowe HM, Jakobsson J, Mesnard D, Rougemont J, Reynard S, Aktas T, et al. KAP1 controls endogenous retroviruses in embryonic stem cells. Nature. 2010;463(7278):237-40.
41. Stieger K, Belbellaa B, Le Guiner C, Moullier P, Rolling F. In vivo gene regulation using tetracycline-regulatable systems. Advanced drug delivery reviews. 2009;61(7-8):527-41.
42. Wolf G, Yang P, Fuchtbauer AC, Fuchtbauer EM, Silva AM, Park C, et al. The KRAB zinc finger protein ZFP809 is required to initiate epigenetic silencing of endogenous retroviruses. Genes & development. 2015;29(5):538-54. PMCID: 4358406.
43. Groner AC, Meylan S, Ciuffi A, Zangger N, Ambrosini G, Denervaud N, et al. KRAB-zinc finger proteins and KAP1 can mediate long-range transcriptional repression through heterochromatin spreading. PLoS genetics. 2010;6(3):e1000869. PMCID: 2832679.
44. Baril P, Pichon C. Positive Bioluminescence Imaging of MicroRNA Expression in Small Animal Models Using an Engineered Genetic-Switch Expression System, RILES. Methods in molecular biology. 2016;1372:193-208.
45. Ezzine S, Vassaux G, Pitard B, Barteau B, Malinge JM, Midoux P, et al. RILES, a novel method for temporal analysis of the in vivo regulation of miRNA expression. Nucleic acids research. 2013;41(20):e192. PMCID: 3814383.
46. Simion V, Sobilo J, Clemoncon R, Natkunarajah S, Ezzine S, Abdallah F, et al. Positive radionuclide imaging of miRNA expression using RILES and the human sodium iodide symporter as reporter gene is feasible and supports a protective role of miRNA-23a in response to muscular atrophy. PloS one. 2017;12(5):e0177492. PMCID: 5426778.
47. Simion V, Henriet E, Juric V, Aquino R, Loussouarn C, Laurent Y, et al. Intracellular trafficking and functional monitoring of miRNA delivery in glioblastoma using lipopolyplexes and the miRNA-ON RILES reporter system. Journal of controlled release : official journal of the Controlled Release Society. 2020;327:429-43.
48. Benabdellah K, Cobo M, Munoz P, Toscano MG, Martin F. Development of an all-in-one lentiviral vector system based on the original TetR for the easy generation of Tet-ON cell lines. PloS one. 2011;6(8):e23734. PMCID: 3158098.
49. Sehedic D, Chourpa I, Tetaud C, Griveau A, Loussouarn C, Avril S, et al. Locoregional Confinement and Major Clinical Benefit of (188)Re-Loaded CXCR4-Targeted Nanocarriers in an Orthotopic Human to Mouse Model of Glioblastoma. Theranostics. 2017;7(18):4517-36. PMCID: 5695146.
50. Denning W, Das S, Guo S, Xu J, Kappes JC, Hel Z. Optimization of the transductional efficiency of lentiviral vectors: effect of sera and polycations. Mol Biotechnol. 2013;53(3):308-14. PMCID: 3456965.
51. Chen JF, Mandel EM, Thomson JM, Wu Q, Callis TE, Hammond SM, et al. The role of microRNA-1 and microRNA-133 in skeletal muscle proliferation and differentiation. Nature genetics. 2006;38(2):228-33. PMCID: 2538576.
52. Yang CH, Yue J, Pfeffer SR, Fan M, Paulus E, Hosni-Ahmed A, et al. MicroRNA-21 promotes glioblastoma tumorigenesis by down-regulating insulin-like growth factor-binding protein-3 (IGFBP3). The Journal of biological chemistry. 2014;289(36):25079-87. PMCID: 4155674.
53. Goncalves C, Berchel M, Gosselin MP, Malard V, Cheradame H, Jaffres PA, et al. Lipopolyplexes comprising imidazole/imidazolium lipophosphoramidate, histidinylated polyethyleneimine and siRNA

as efficient formulation for siRNA transfection. International journal of pharmaceutics. 2014;460(1-2):264-72.
54. Bramsen JB, Laursen MB, Nielsen AF, Hansen TB, Bus C, Langkjaer N, et al. A large-scale chemical modification screen identifies design rules to generate siRNAs with high activity, high stability and low toxicity. Nucleic acids research. 2009;37(9):2867-81. PMCID: 2685080.
55. Rana TM. Illuminating the silence: understanding the structure and function of small RNAs. Nature reviews Molecular cell biology. 2007;8(1):23-36.
56. Yoshioka K, Kunieda T, Asami Y, Guo H, Miyata H, Yoshida-Tanaka K, et al. Highly efficient silencing of microRNA by heteroduplex oligonucleotides. Nucleic acids research. 2019;47(14):7321-32. PMCID: 6698647.
57. Hu HY, Yan Z, Xu Y, Hu H, Menzel C, Zhou YH, et al. Sequence features associated with microRNA strand selection in humans and flies. BMC Genomics. 2009;10:413. PMCID: 2751786.
58. Pierce RL. Translational nanomedicine--through the therapeutic window. Nanomedicine (Lond). 2015;10(21):3249-60.
59. Cooney L, Loke YK, Golder S, Kirkham J, Jorgensen A, Sinha I, et al. Overview of systematic reviews of therapeutic ranges: methodologies and recommendations for practice. BMC Med Res Methodol. 2017;17(1):84. PMCID: 5455119.
60. Saucier-Sawyer JK, Seo YE, Gaudin A, Quijano E, Song E, Sawyer AJ, et al. Distribution of polymer nanoparticles by convection-enhanced delivery to brain tumors. Journal of controlled release : official journal of the Controlled Release Society. 2016;232:103-12. PMCID: 4893898.
61. Mehta AM, Sonabend AM, Bruce JN. Convection-Enhanced Delivery. Neurotherapeutics : the journal of the American Society for Experimental NeuroTherapeutics. 2017;14(2):358-71. PMCID: 5398992.
62. Seo YE, Bu T, Saltzman WM. Nanomaterials for convection-enhanced delivery of agents to treat brain tumors. Current opinion in biomedical engineering. 2017;4:1-12. PMCID: 5761746.
63. Engin AB, Nikitovic D, Neagu M, Henrich-Noack P, Docea AO, Shtilman MI, et al. Mechanistic understanding of nanoparticles' interactions with extracellular matrix: the cell and immune system. Part Fibre Toxicol. 2017;14(1):22. PMCID: 5483305.
64. Khawar IA, Kim JH, Kuh HJ. Improving drug delivery to solid tumors: priming the tumor microenvironment. Journal of controlled release : official journal of the Controlled Release Society. 2015;201:78-89.
65. Dzobo K, Senthebane DA, Thomford NE, Rowe A, Dandara C, Parker MI. Not Everyone Fits the Mold: Intratumor and Intertumor Heterogeneity and Innovative Cancer Drug Design and Development. OMICS. 2018;22(1):17-34.
66. Sagnella SM, McCarroll JA, Kavallaris M. Drug delivery: beyond active tumour targeting. Nanomedicine. 2014;10(6):1131-7.
67. Dagogo-Jack I, Shaw AT. Tumour heterogeneity and resistance to cancer therapies. Nat Rev Clin Oncol. 2018;15(2):81-94.
68. Ipas H, Guttin A, Issartel JP. Exosomal MicroRNAs in Tumoral U87 MG Versus Normal Astrocyte Cells. Microrna. 2015;4(2):131-45.
69. Luhtala N, Aslanian A, Yates JR, 3rd, Hunter T. Secreted Glioblastoma Nanovesicles Contain Intracellular Signaling Proteins and Active Ras Incorporated in a Farnesylation-dependent Manner. The Journal of biological chemistry. 2017;292(2):611-28. PMCID: 5241736.
70. Zhang B, Pan X, Cobb GP, Anderson TA. microRNAs as oncogenes and tumor suppressors. Dev Biol. 2007;302(1):1-12.
71. Frixa T, Donzelli S, Blandino G. Oncogenic MicroRNAs: Key Players in Malignant Transformation. Cancers (Basel). 2015;7(4):2466-85. PMCID: 4695904.
72. Mutlu M, Raza U, Saatci O, Eyupoglu E, Yurdusev E, Sahin O. miR-200c: a versatile watchdog in cancer progression, EMT, and drug resistance. J Mol Med (Berl). 2016;94(6):629-44.

73. Kumar S, Nag A, Mandal CC. A Comprehensive Review on miR-200c, A Promising Cancer Biomarker with Therapeutic Potential. Current drug targets. 2015;16(12):1381-403.
74. Huse JT, Holland EC. Targeting brain cancer: advances in the molecular pathology of malignant glioma and medulloblastoma. Nat Rev Cancer. 2010;10(5):319-31.
75. Hatoum A, Mohammed R, Zakieh O. The unique invasiveness of glioblastoma and possible drug targets on extracellular matrix. Cancer management and research. 2019;11:1843-55. PMCID: 6395056.
76. Feng X, Wang Z, Fillmore R, Xi Y. MiR-200, a new star miRNA in human cancer. Cancer letters. 2014;344(2):166-73. PMCID: 3946634.
77. Qin Y, Chen W, Liu B, Zhou L, Deng L, Niu W, et al. MiR-200c Inhibits the Tumor Progression of Glioma via Targeting Moesin. Theranostics. 2017;7(6):1663-73. PMCID: 5436519.
78. Mirimanoff RO, Gorlia T, Mason W, Van den Bent MJ, Kortmann RD, Fisher B, et al. Radiotherapy and temozolomide for newly diagnosed glioblastoma: recursive partitioning analysis of the EORTC 26981/22981-NCIC CE3 phase III randomized trial. J Clin Oncol. 2006;24(16):2563-9.
79. Koo T, Cho BJ, Kim DH, Park JM, Choi EJ, Kim HH, et al. MicroRNA-200c increases radiosensitivity of human cancer cells with activated EGFR-associated signaling. Oncotarget. 2017;8(39):65457-68. PMCID: 5630345.

Figure

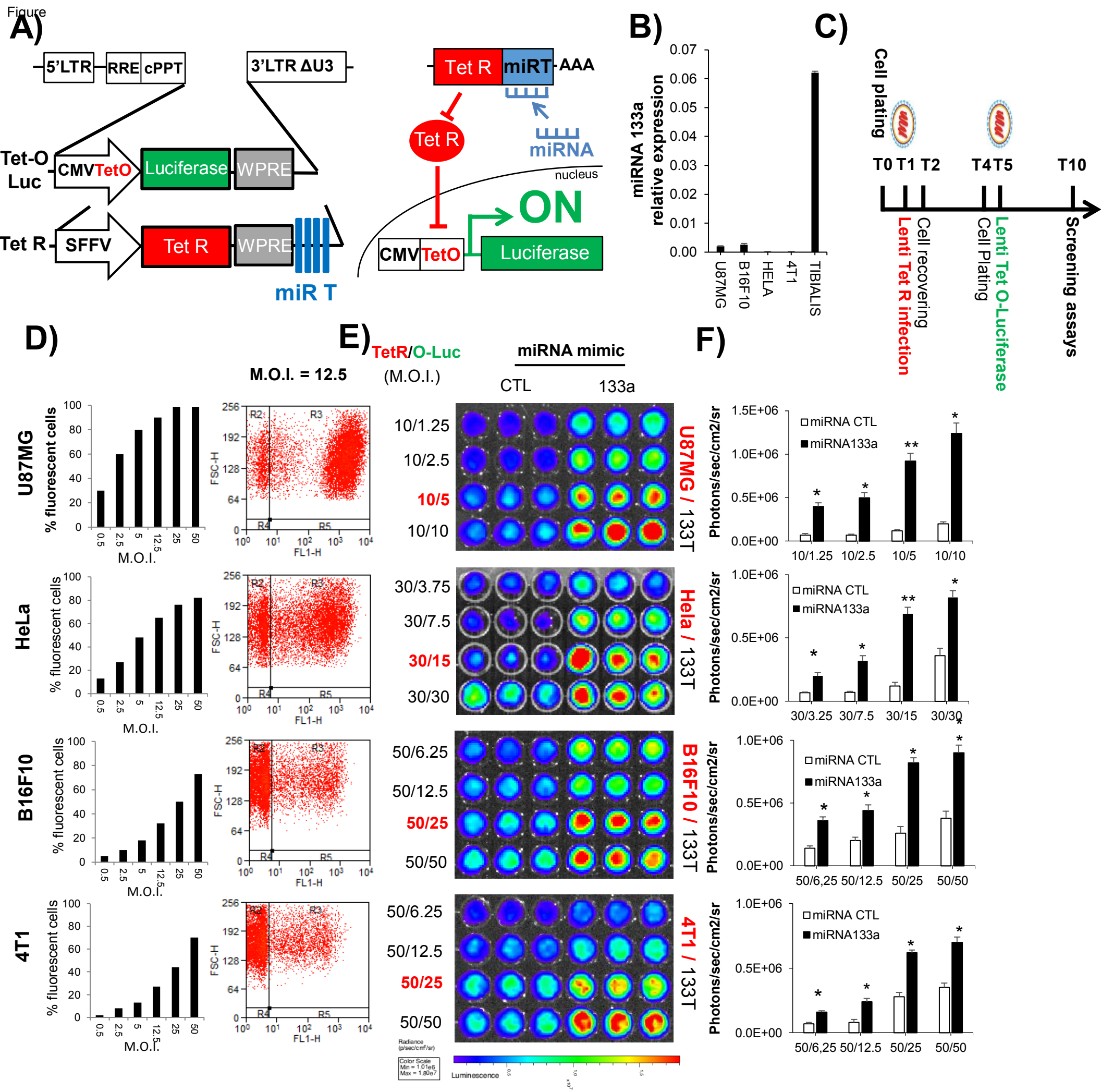

Figure 1. Schematic representation of the lentiRILES system and strategy to generate miRNA-responsive stable cell lines.

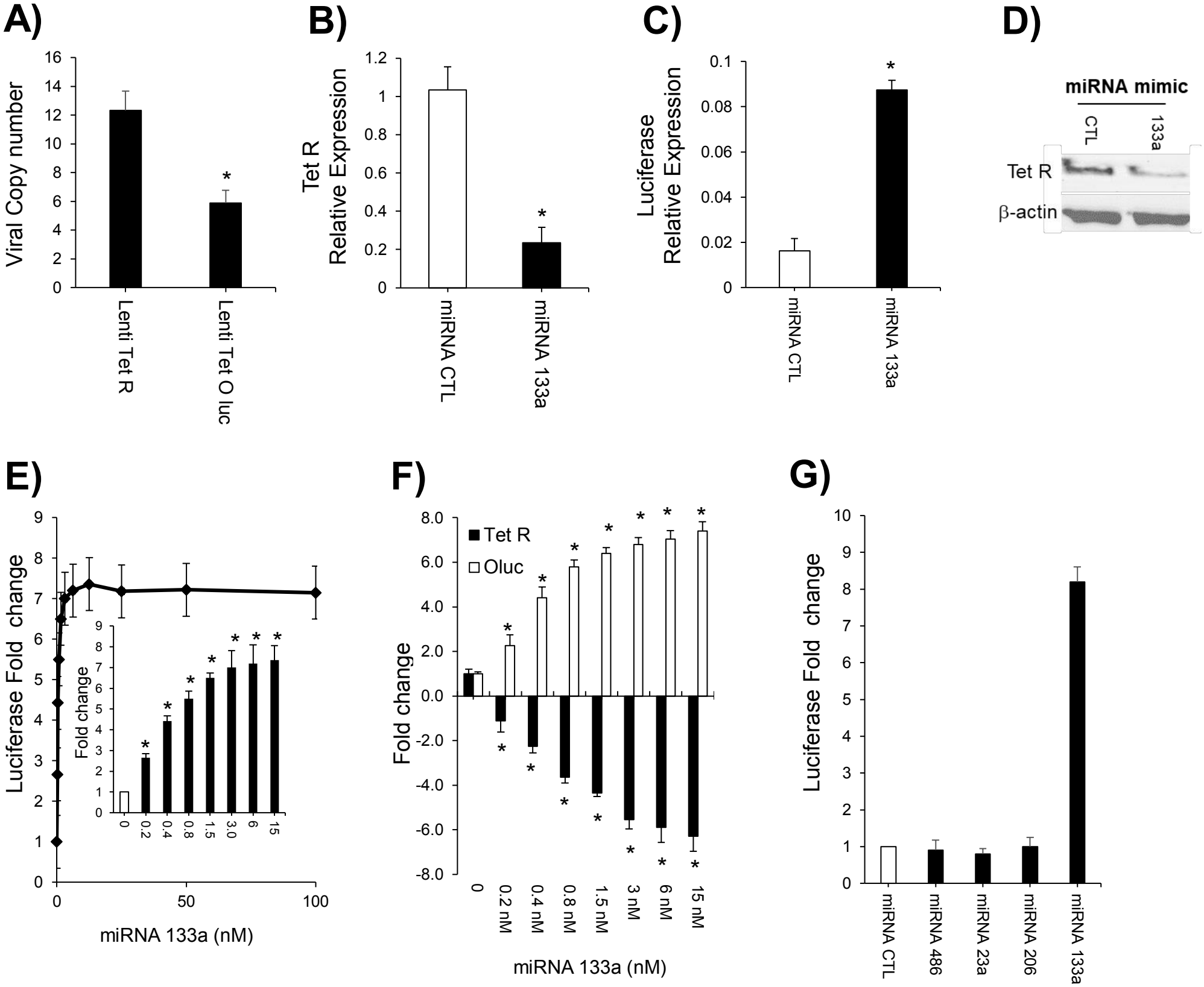

Figure 2. Molecular characterization of the OFF-to-ON shift of the RILES/133T stably integrated in the genome of the LentiRILES U87MG/133T cell line.

C2C12

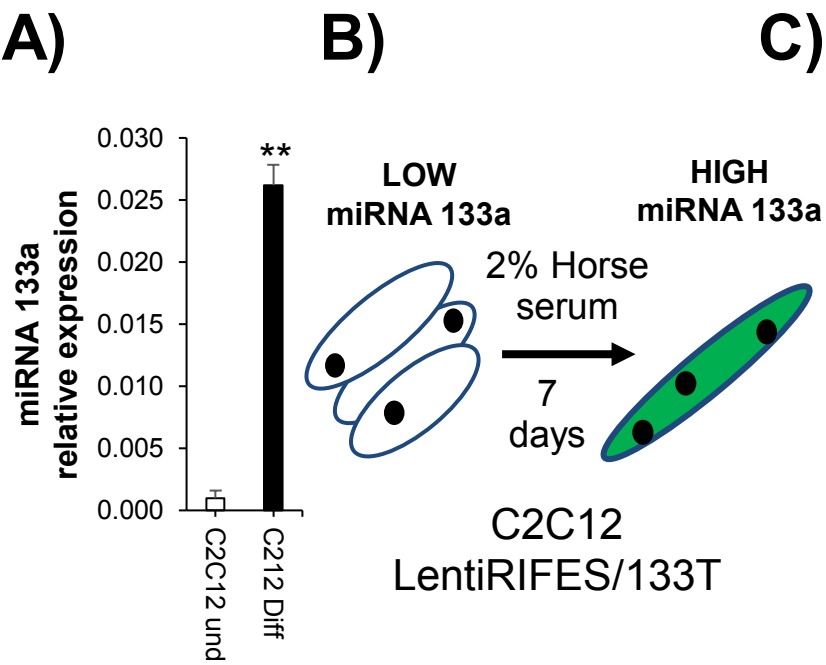

U87MG

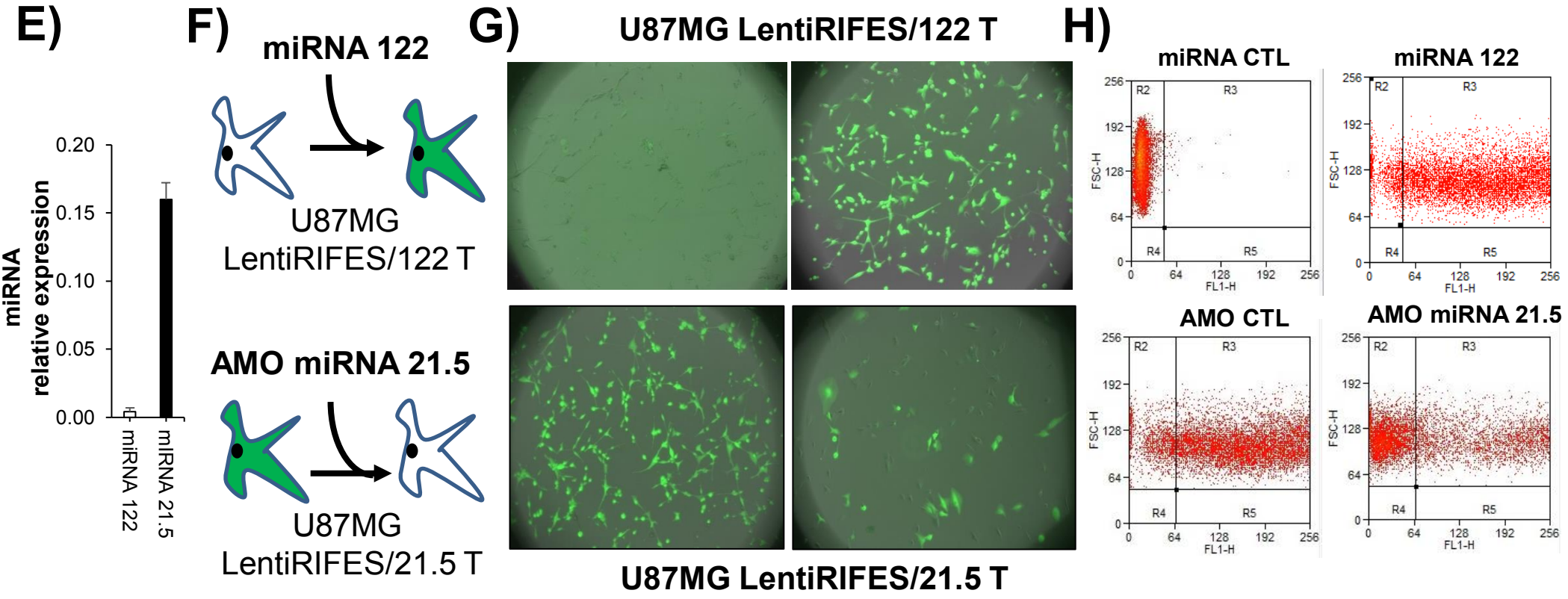

Figure 3. Real time, fluorescence monitoring of endogenously expressed miRNA in cell lines.

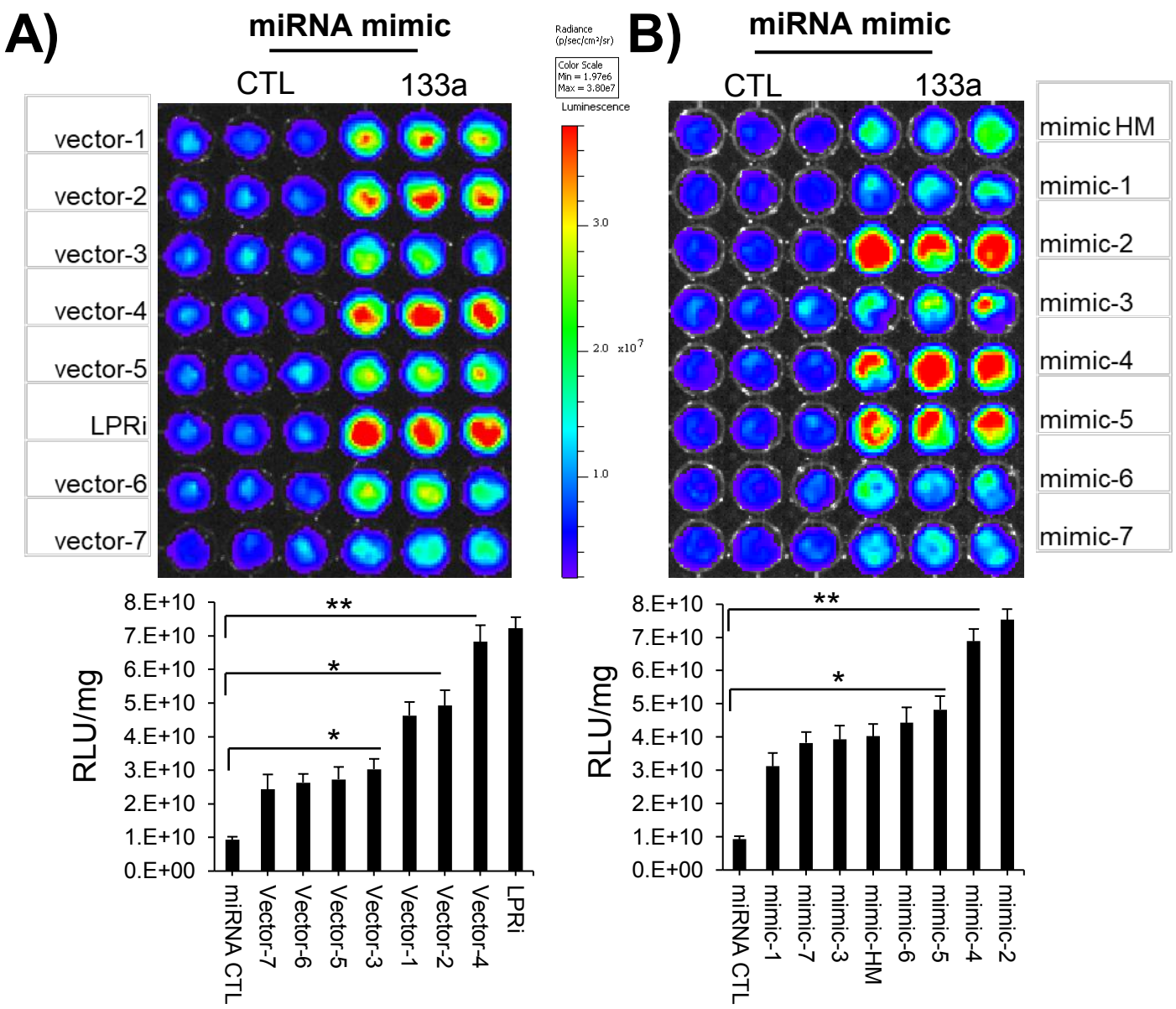

Figure 4. Cell-based miRNA screening platform using the U87MG LentiRILES/133T cell line.

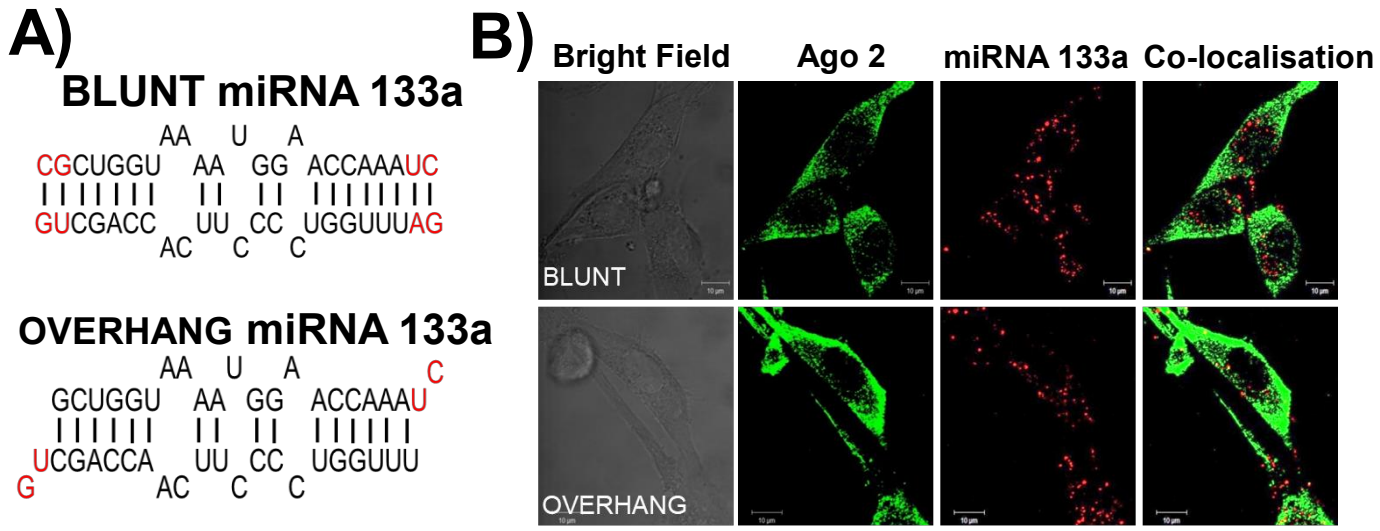

Figure 5. Structure and function relationship study of miRNA-133a duplexes using the U87MG LentiRILES/133T cell line

A)

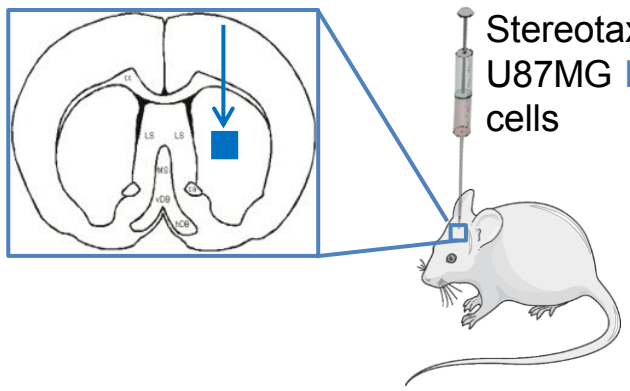

B)

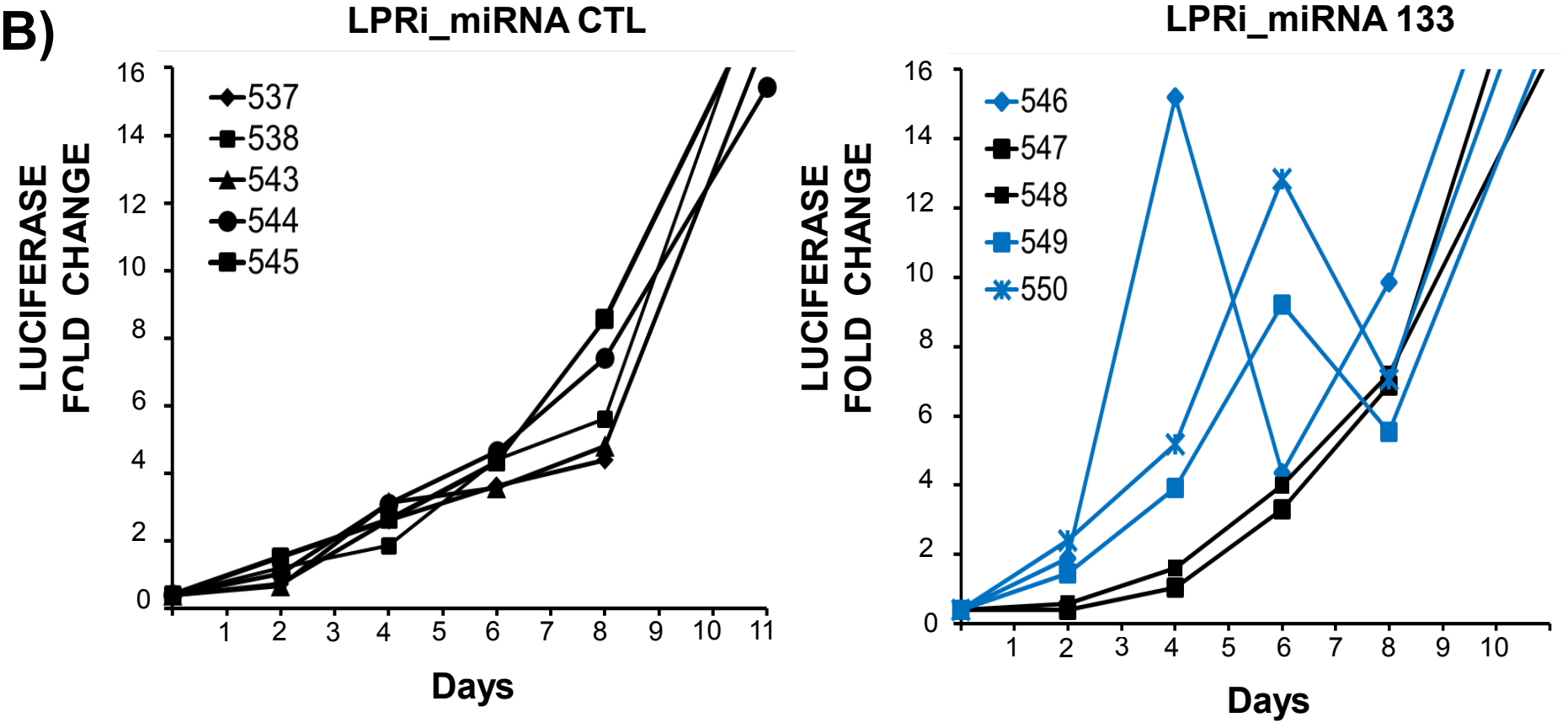

C)

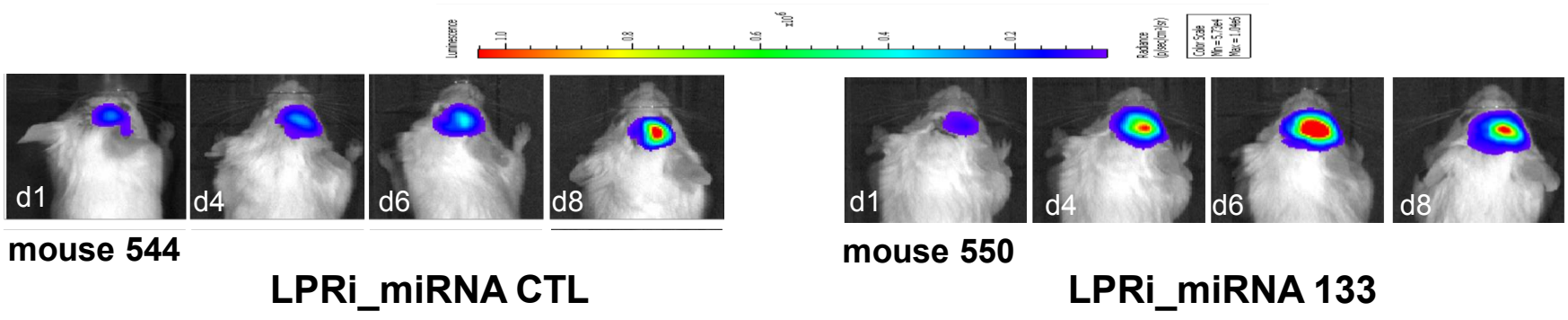

Figure 6. *In vivo* bioluminescence monitoring of kinetic of miRNA-133a activity following intracranial delivery in an orthotopic glioblastoma mouse model

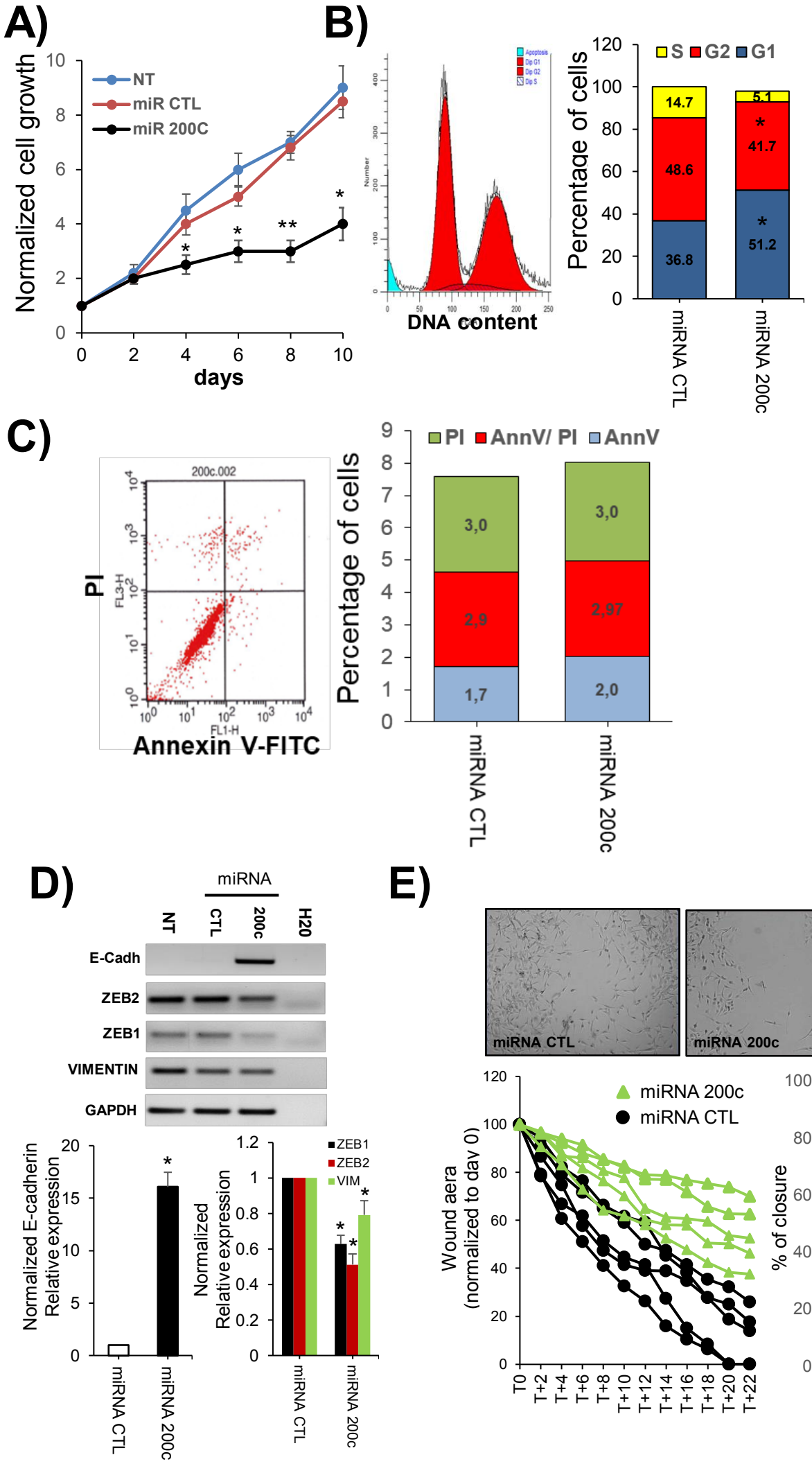

Figure 7. Tumour suppressive function evaluation of miRNA-200c in U87MG cells *in vitro*

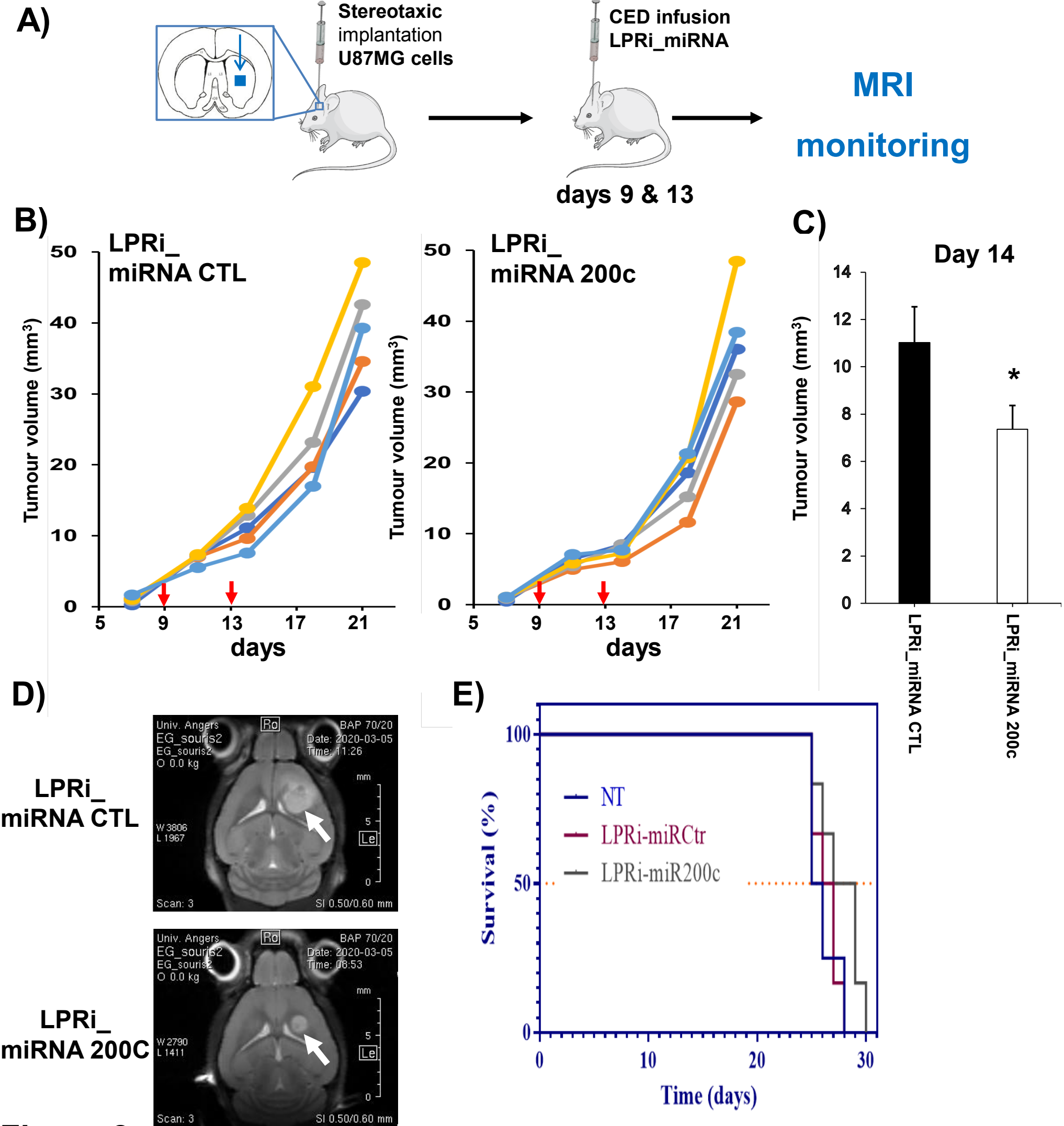

Figure 8 Tumour suppressive evaluation of miRNA-200c in a preclinical animal model of glioblastoma